Passive Seismic Characterization of High Priority Salt Jugs in Hutchinson, Kansas: April 2025

Shelby L. Peterie, Julian Ivanov, Marcus Tamburro, Richard D. Miller,
Brett Wedel, Robbie Kieffer, Connor Umbrell, Cole Bunker, and Carl Gonzales

Kansas Geological Survey
1930 Constant Avenue
Lawrence, KS 66047

Report to

Dale Davis and Spencer Cronin
Burns & McDonnell
9400 Ward Parkway
816-839-9526

Open-file Report 2025–62 June 2025

The Kansas Geological Survey makes no warranty or representation, either express or implied, with regard to the data, documentation, or interpretations or decisions based on the use of this data including the quality, performance, merchantability, or fitness for a particular purpose. Under no circumstances shall the Kansas Geological Survey be liable for damages of any kind, including direct, indirect, special, incidental, punitive, or consequential damages in connection with or arising out of the existence, furnishing, failure to furnish, or use of or inability to use any of the database or documentation whether as a result of contract, negligence, strict liability, or otherwise. This study was conducted in complete compliance with ASTM Guide D7128-05. All data, interpretations, and opinions expressed or implied in this report and associated study are reasonably accurate and in accordance with generally accepted scientific standards.

Passive Seismic Characterization of High Priority Salt Jugs in Hutchinson, Kansas: April 2025

Executive Summary

This project appraised changes in stress conditions of rock above selected dissolution voids by estimating the relative stress field from the calculated shear-wave velocity of the overburden. An estimate of change and potential risk each void represents can be estimated by comparing the current stress conditions with those measured in previous surveys. Shear-wave velocities were calculated using passive surface-wave methods. Data were acquired along thirteen profiles located on or near key abandoned brine production wells using train traffic as an energy source. The multichannel analysis of surface waves (MASW) method provided an estimate of the shear-wave velocity, at a resolution sufficient to loosely map the alluvial/bedrock contact and velocity characteristics of the Permian-aged Ninnescah Shale above the top of the "three finger" dolomite (at approximately 100 m below ground surface). A key outcome was the differentiation of relative rock stress based on shear velocity above solution mining caverns (salt jugs, associated with the target wells) compared to rocks above undisturbed salt or jugs reported without wide spans of unsupported roof rock. Comparisons of shear-wave velocity profiles over time (timelapse) provided insights into consistency of overburden stability and therefore, indirectly, void dynamics.

Passive MASW data were continuously acquired over four nights (April 14–17, 2025) above wells with a potential to impact surface access or assets or with production histories consistent with past cases of void migration on the Vigindustries site in Hutchinson, Kansas. A continuous sampling approach targeting different wells each night was used to record all available train sources of passive source energy to maximize opportunities to capture energy with optimal source orientation and surface-wave characteristics. Surface waves were recorded with frequencies as low as 4.5 Hz, representing an approximately 60 m average maximum depth of investigation, and used to map bedrock velocity of at least the upper 40 m.

Since shear modulus is the ratio of stress over strain and shear-wave velocity is a function of shear modulus and density, it is possible to estimate relative stress of overburden rocks (shear modulus) from shear-wave velocity values. Local increases in shear-wave velocity above background and without correlation to changes in lithology can be equated to increases in stress associated with changes in the distribution of overburden roof rock loading above solution jugs. Relative shear-wave velocity lows may be associated with remnants of a partial or incremental collapse whose vertical movement has been arrested by bulking, reduction in overburden stress due to changes in void geometry resulting in stress redistribution within roof rock, or changes in rock strength due to different geologic properties related to natural variation.

Overall, shear-wave velocity directly over or in proximity to most of the 47 wells in this year's study is consistent with natural geologic conditions and a normal stress regime as observed in previous years' studies. Results suggest the shale overburden across the site is currently in a state of relative stability with localized changes suggesting possible future stress redistribution (which could include vertical migration) at less than a dozen wells. Overburden materials at or near seven wells from this April 2025 survey were interpreted to have subtle but notable changes in overburden characteristics relative to past years or native material properties. Bedrock velocity at well 2A, a major focus of past reports due to dynamic overburden conditions and possible limited failure at depth, experienced a 30% reduction in velocity along line 10,

suggesting dynamic changes continue in this area. In addition, timelapse variability may suggest dynamic stress changes associated with changes in roof structures or characteristics of salt jugs have occurred near wells 3B, 6B, 7B, 8A, 52, and 53. Apparent shear-wave velocity at these wells is slightly elevated compared to previous surveys, possibly representing increased stress at depth. The relatively small velocity increases do not appear to suggest an imminent threat of vertical migration at this time. Follow-up surveys are recommended on an annual basis.

Introduction

Material properties (specifically stress accumulations) measured as a function of depth above abandoned salt jugs in Hutchinson, Kansas, appear related to the load density associated with the tensional dome of these jugs. Localized escalation in stress (as indicated by increased shear-wave velocity) above subterranean voids is one indicator of an increased potential for roof failure and void migration (Eberhart-Phillips et al., 1989; Dvorkin et al., 1996; Khaksar et al., 1999; Sayers, 2004). Previous studies, using both active and passive seismic wavefield characteristics, suggest perturbations in the shear-wave velocity field immediately above voids can be correlated to characteristics of the unsupported roof spans of salt jugs in the Hutchinson area (Sloan et al., 2010).

The strength of individual rock layers can be qualitatively described in terms of stiffness/ rigidity and empirically estimated from relative comparisons of shear-wave velocity measurements. Shear-wave velocity is directly proportional to stress and inversely related to non-elastic strain. Since the shear-wave velocity of earth materials changes when stress and any associated elastic strain on those materials becomes "large," it is reasonable to suggest load-bearing roof rock above mines or dissolution voids may experience elevated shear-wave velocities due to loading between pillars or, in the case of voids, loading between supporting side walls. This localized increase in shear velocity is not related to increased strength but to increased load as defined by Young's Modulus. High-velocity shear-wave encompassing low-velocity anomalies ("halo" anomalies) are suggested to be key indicators of near-term roof failure. All these phenomena have been observed within the overburden above voids in the Hutchinson Salt Member in Hutchinson at depths greater than 30 m below the bedrock surface.

Previous research projects at the Carey Boulevard Research Area (CBRA) correlated measured shear-wave velocities with the condition of dissolution void roofs and the physical properties of the overburden at selected locations on Vigindustries legacy solution mining property in Hutchinson. In 2008, active seismic reflection was used to evaluate the effectiveness of shear-wave velocity as a relative measure of local stress above voids representative (in the size and depth) of those prevalent at the Vigindustries site (Miller et al., 2009). It was determined that the integrity of the overlying strata could be reasonably estimated using shear-wave seismic reflection imaging. The lack of necessary ultra-low-frequency surface waves in the recorded wavefield negated attempts to use active-source multi-channel analysis of surface waves (MASW) to estimate shear velocity in the lithified rocks above the voids and near the top of bedrock (Miller et al., 2009).

Uncontrolled local industrial and transportation activities represent sound sources that can produce the necessary low frequency seismic waves to interrogated rock material at depth greater than 60 m using passive methods (Miller, 2011). Key to this method is the ability to estimate shear-wave velocities using MASW to depths more than double those possible using standard active sources (Park et al., 2004). Results of passive MASW studies at and near this

site suggest that this method is effective in identifying jugs with heightened risk for upward migration (Miller, 2011; Ivanov et al., 2013).

Following the active seismic imaging study in 2008, two-dimensional (2-D) passive MASW surveys have been acquired at the Vigindustries site since 2012 to appraise the stability/consistency of overburden at selected wells (Table 1). Results of these investigations suggested a normal stress regime with natural geologic variation above most wells. Shear velocity above a few wells was noted to be outside what might be considered normal for the area and justified more attention. Individually, each profile represents a snapshot in time. When combined with previous observations at the same locations, timelapse analysis can be used to monitor temporal variation in shear velocity, providing insight into relative stability and void dynamics.

Table 1. Dates of wells evaluated during 2-D passive MASW surveys at the CBRA.

Date	Wells
August 2012	2A, 1B, 2B, 3B, 5B, 6B, 7B, 12B
October 2012	2B, 4B, 6B, 17, 45, 52, 53, 59
March 2013	2A, 4B
November 2014	2A, 3B, 4B
March 2015	1B, 2B, 3B, 6B, 8A, 8B, 10B, 11B, 12B, 13B, 14B, 15B, 17, 18, 22A, 23, 23B, 29, 30, 39, 41, 42, 44, 45, 46, 86, 87, 88, 89, 90, 92
May 2015	2A, 4B
June 2015	4A, 6B, 7A, 7B, 52, 53, 59, 60
November 2017	2A, 4A, 7A, 8A, 1B, 2B, 3B, 4B, 6B, 7B, 8B, 10B, 11B, 12B, 13B, 14B, 15B, 17, 18, 22A, 23, 23B, 29, 30, 39, 41, 42, 44, 45, 46, 52, 53, 59, 60, 86, 87, 88, 89, 90, 92
October 2018	2A, 4B
December 2018	1B, 2B, 3B, 4A, 4B, 6B, 7A, 7B, 8A, 8B, 10B, 11B, 12B, 13B, 14B, 15B, 17, 18, 22A, 23B, 23, 29, 30, 39, 41, 42, 44, 45, 46, 52, 53, 59, 60, 86, 87, 88, 89, 90
December 2019	1B, 2A, 2B, 3B, 4A, 4B, 5B, 6B, 7A, 7B, 8A, 8B, 10B, 11B, 12B, 13B, 14B, 15B, 17, 18, 22A, 23B, 23, 29, 30, 39, 42, 44, 45, 46, 52, 53, 59, 60, 88, 89, 90, 92
August 2020	2A, 4A, 7A, 15B, 59
November 2020	1B, 2A, 2B, 3B, 4A, 4B, 5B, 6B, 7A, 7B, 8A, 8B, 10B, 11B, 12B, 13B, 14B, 15B, 17, 18, 22A, 23B, 23, 29, 30, 39, 42, 44, 45, 46, 52, 53, 59, 60, 88, 89, 90, 92
November 2021	1B, 2A, 2B, 3B, 4A, 4B, 5B, 6B, 7A, 7B, 8A, 8B, 10B, 11B, 12B, 13B, 14B, 15B, 17, 18, 19, 20, 22A, 23B, 23, 25, 26, 29, 30, 33, 36, 39, 41, 42, 44, 45, 46, 52, 53, 59, 60, 88, 89, 90, 92, 94
March 2023	1B, 2A, 2B, 3B, 4A, 4B, 5B, 6B, 7A, 7B, 8A, 8B, 10B, 11B, 12B, 13B, 14B, 15B, 17, 18, 19, 20, 22A, 23B, 23, 25, 26, 29, 30, 33, 36, 39, 41, 42, 44, 45, 46, 52, 53, 59, 60, 88, 89, 90, 92, 94
November 2023	2A, 4B
August 2024	1B, 2A, 2B, 3B, 4A, 4B, 5B, 6B, 7A, 7B, 8A, 8B, 10B, 11B, 12B, 13B, 14B, 15B, 17, 18, 19, 20, 22A, 23B, 23, 25, 26, 29, 30, 33, 36, 39, 41, 42, 44, 45, 46, 52, 53, 59, 60, 87, 88, 89, 90, 92, 94
April 2025	1B, 2A, 2B, 3B, 4A, 4B, 5B, 6B, 7A, 7B, 8A, 8B, 10B, 11B, 12B, 13B, 14B, 15B, 17, 18, 19, 20, 22A, 23B, 23, 25, 26, 29, 30, 33, 36, 39, 41, 42, 44, 45, 46, 52, 53, 59, 60, 87, 88, 89, 90, 92, 94

Geologic and Geophysical Setting

The Permian-aged Hutchinson Salt Member occurs in central Kansas, northwestern Oklahoma, and the northeastern portion of the Texas panhandle and is prone to and has an extensive history of dissolution and formation of sinkholes (Figure 1). In Kansas, the Hutchinson Salt Member possesses an average net thickness of 75 m and reaches a maximum of more than 150 m in the southern part of the basin. Deposition occurring during fluctuating sea levels caused numerous halite beds, 0.2 to 3 m thick, to be formed interbedded with shale, minor anhydrite, and dolomite/magnesite. Individual salt beds may be continuous for only a few miles despite the remarkable lateral continuity of the salt as a whole (Walters, 1978).

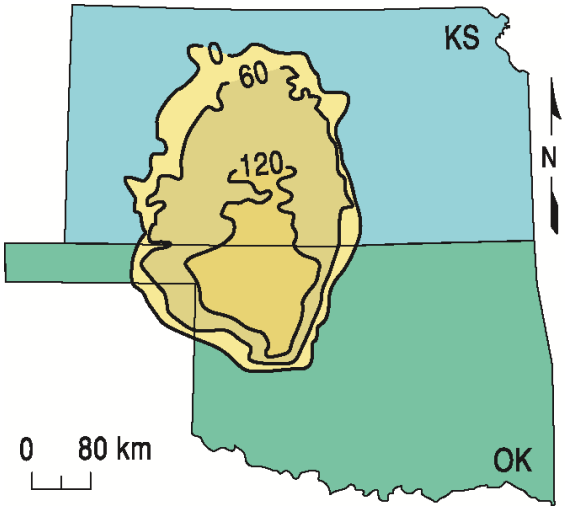

Figure 1. Approximate extent of salt formation, with contour intervals expressed in meters.

The distribution and stratigraphy of the salt is well documented (Dellwig, 1963; Holdoway, 1978; Kulstad, 1959; Merriam, 1963). The salt reaches a maximum thickness in central Oklahoma and thins to depositional edges on the north and west, erosional subcrop on the east, and facies changes on the south. The increasing thickness toward the center of the salt bed is due to a combination of increased salt and more and thicker interbedded anhydrites. The Stone Corral Formation (a well-documented seismic marker bed) overlies the salt throughout Kansas (McGuire and Miller, 1989). Directly above the salt at this site is a thick sequence of Permian shale overlain by a saturated interval of Pliocene-Pliestocene sediments.

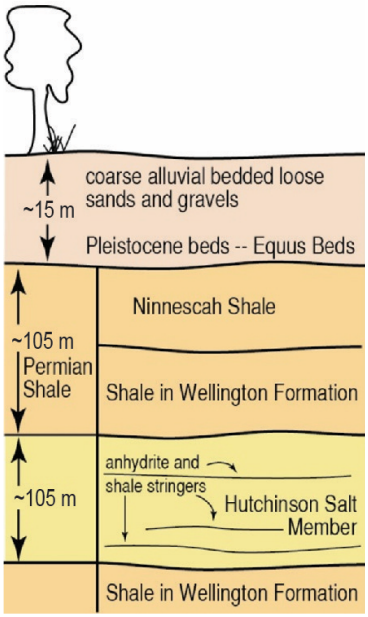

Figure 2. Generalized geology.

The upper 760 m of rock at this site is Permian shale (Merriam, 1963). The lower Wellington Shale (top at ~225 m deep), Hutchinson Salt (top at ~120 m deep), upper Wellington Shale (top at ~70 m deep), and Ninnescah Shale (top at ~15 m deep) make up the Permian portion of the section (Figure 2). Bedrock is defined as the top of the Ninnescah Shale with the unconsolidated Pliocene-Pleistocene Equus beds making up the majority of the upper 15 m of sediment. The thickness of Quaternary alluvium that fills the stream valleys and paleosubsidence features goes from 0 to as much as 90 m, depending on the dimensions of the features.

Recent dissolution of the salt and resulting subsidence of overlying sediments forming sinkholes has generally been associated with mining or saltwater disposal (Walters, 1978). Historically, these sinkholes can manifest themselves as a risk to surface infrastructure. The rate

of surface subsidence can range from gradual to very rapid. Besides risks to surface structures, subsidence features potentially jeopardize the natural segregation of groundwater aquifers, greatly increasing their potential to negatively impact the environment (Whittemore, 1989, 1990). Natural sinkholes resulting from dissolution of the salt by localized leaching within natural flow systems that have been altered by structural features (such as faults and fractures) are not uncommon west of the main dissolution edge (Merriam and Mann, 1957).

Caprock and its characteristics are a very important component of any discussion concerning dissolution, subsidence, and formation of sinkholes. The Permian shales (Wellington and Ninnescah) that overlie the Hutchinson Salt Member are highly variable and can range from less than 60 m to more than 100 m thick in this area and are characterized as generally unstable when exposed to freshwater, being susceptible to sloughing and collapse (Swineford, 1955). These Permian shales tend to be red or reddish-brown and are commonly referred to as "red beds." Permian red beds are extremely impermeable to water and have provided an excellent seal between the freshwaters of the Equus beds and the extremely water-soluble Hutchinson Salt Member. The modern-day expanse and mere presence of the Hutchinson Salt is due to the protection from freshwater provided by these red beds.

Isolating the basal contact of the upper Wellington Formation provides key insights into the general strength of roof rock expected, if dissolution-mined salt jugs reach the top of the salt zone. Directly above the salt/shale contact is approximately 6 m thick dark-colored shale with joint and bedding cracks filled with red halite (Walters, 1978). Once unsaturated brine contacts this shale layer, these red halite-filled joints and bedding planes are rapidly leached, leaving an extremely structurally weak layer.

Field Layout and Data Acquisition

To ensure the highest quality (e.g., signal-to-noise ratio, S/N) data and maximum crew safety, receivers were deployed during daylight hours, and train data were recorded at night when cultural and industrial noise was minimal, thereby providing the highest possible S/N. Analysis of previous seismic energy sources captured during passive recording at this site clearly indicated trains at distances of 2 kilometers (km) or more provided the best broad spectrum, low-frequency seismic energy (Miller, 2011). Since seismic energy with characteristics best suited for this study may arrive when trains are at distances greater than can be detected by spotters, seismic energy was recorded continuously throughout the night to capture all times, ensuring optimum data.

Data were acquired April 14–18, 2025. A total of thirteen seismic lines (Figure 3) were deployed during the day over this four-day period. Line layout was designed to cross directly over wells of interest. A 2-D square grid of receivers was recorded simultaneously to allow determination of the incident orientation of passive seismic energy. Seismic receivers were single ION 4.5 Hz geophones spaced at 3 m intervals. The westernmost 5 geophones on line 10 were located on the road used to access the grain elevator, requiring rock plates instead of steel spikes. The seismic lines collectively totaled approximately 5000 m in length. The 2-D monitoring/alignment grid consisted of 128 receivers spaced at 5 m intervals and was configured to form four concentric expanding squares with 10, 30, 50, and 70 m sides (Figure 4). Data were recorded with a 400+ channel 24-bit Geometrics Geode distributed seismic system. Line 15 and the 2-D grid utilized a wireless nodal acquisition system by GTI that recorded output from the

geophones. Seismic records from the Geometrics system were 30 seconds (s) long with a 2 millisecond (ms) sampling interval. In total, 3124 seismic records were recorded.

Processing and Analysis

Data were processed using algorithms developed at the Kansas Geological Survey (KGS). The passive method used for this study is well published and has consistently proven effective, producing good-quality results in other studies (Park et al., 2004; Ivanov et al., 2013). The continuous-data-acquisition method records energy from nearby sources at various orientations with respect to the seismic line. Data from the 2-D grid are evaluated for optimized source alignment with respect to each 1-D seismic line allowing data rotation and analysis or direct analysis of only data from near in-line sources.

For each line, the surface-wave amplitudes recorded by the 2-D grid were plotted as phase velocity versus frequency across a range of azimuths (0 to 360 degrees) (Figure 5), relative to the seismic line. This display was effective for identifying the best broad-band, low-frequency source energy with an azimuth as near zero as possible. Seismograms for each line were selected and segmented into the shortest groups of receivers ("spread length") with optimum source characteristics that resulted in dispersion patterns on phase velocity versus frequency plots with the greatest percentage of high-amplitude fundamental-mode Rayleigh-wave energy and minimal higher-order surface-wave interference (Figure 6).

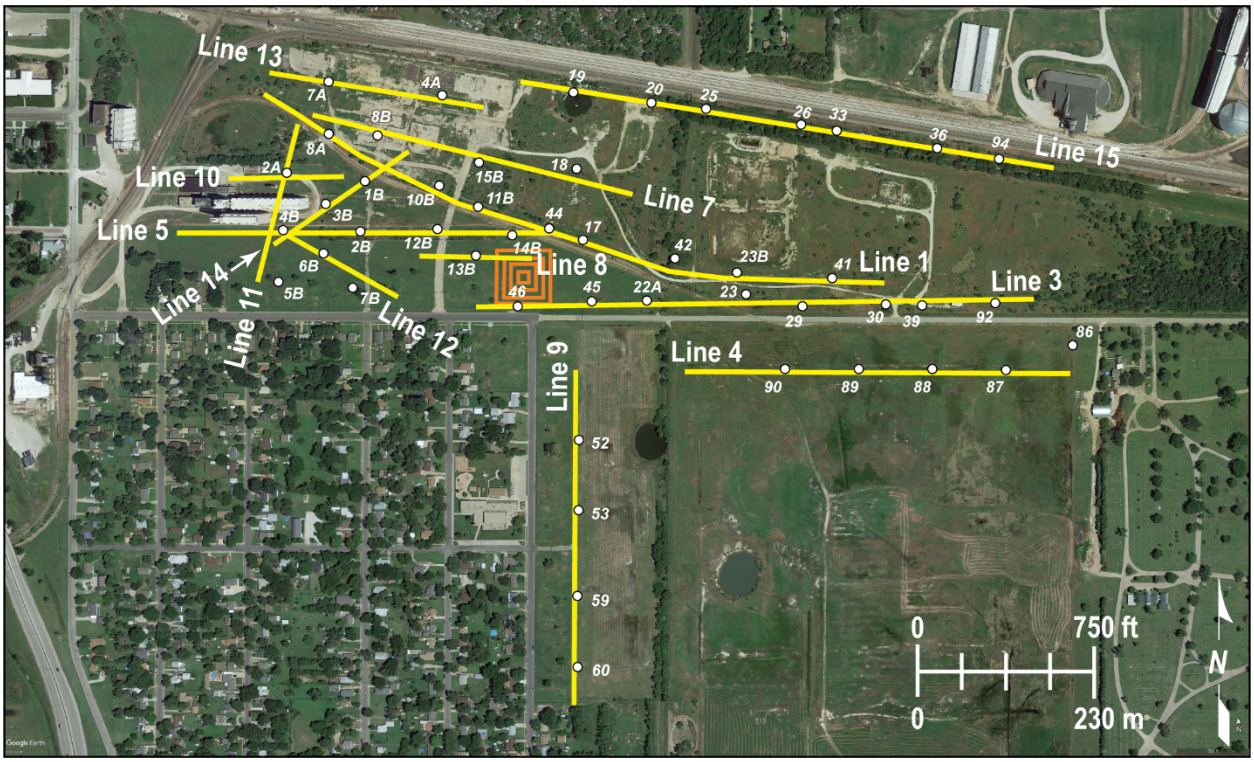

Figure 3. Aerial photo with GPS locations of thirteen seismic lines, 2-D grid of receivers (orange squares), and wells in the November 2021 study.

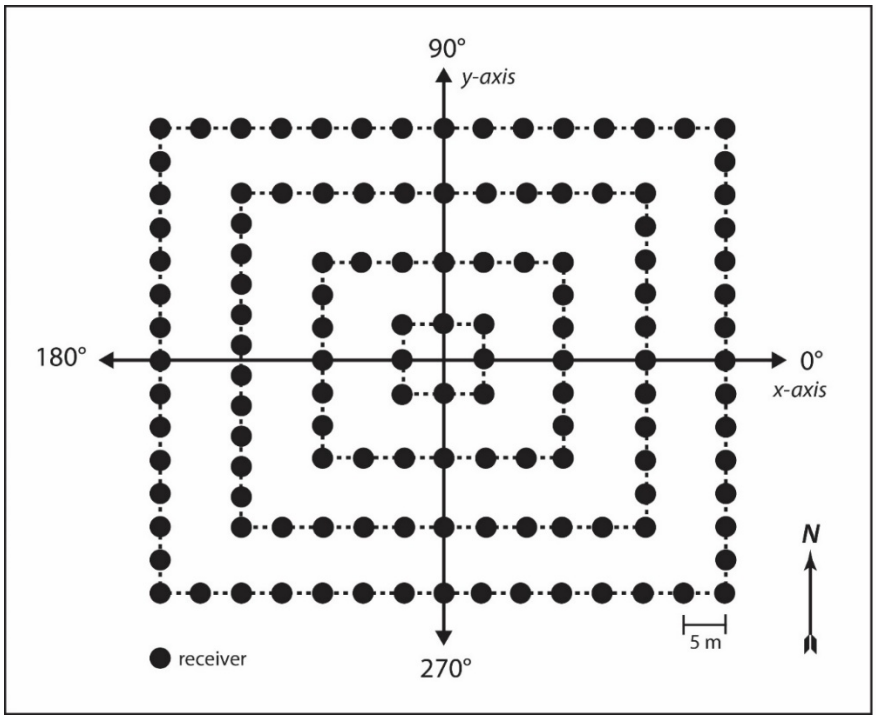

Figure 4. Four nested square arrays were deployed each night to construct the 2-D square grid for determining incident source azimuth information.

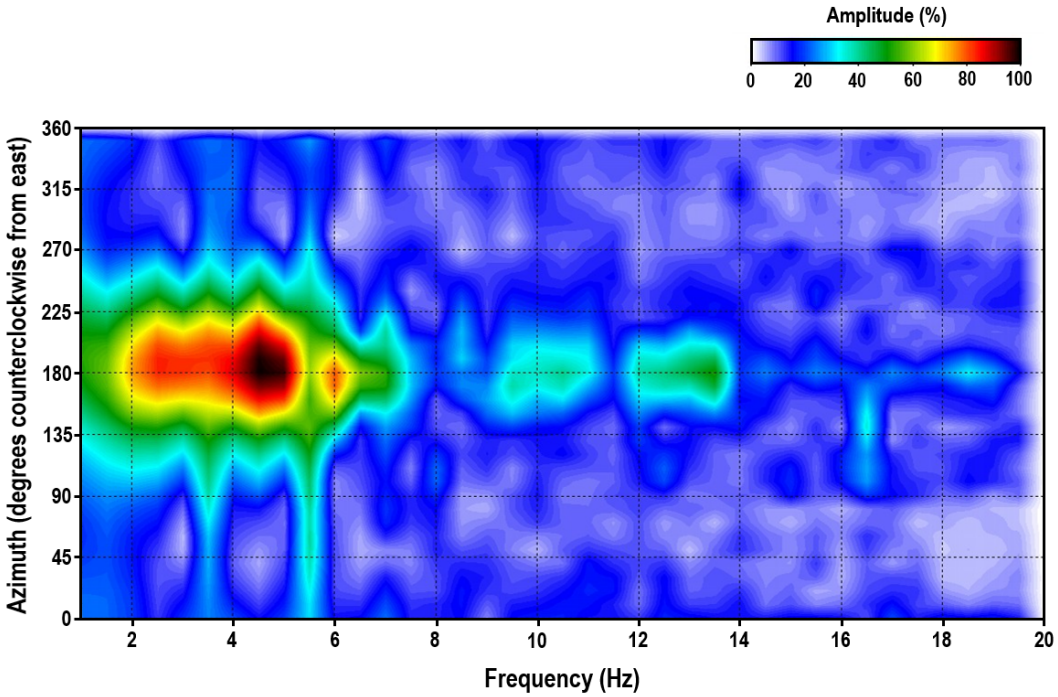

Figure 5. Azimuth plot indicating the direction of the dominant passive source energy (in degrees counter-clockwise from east). Here, the dominant passive source energy is centered on approximately 180°.

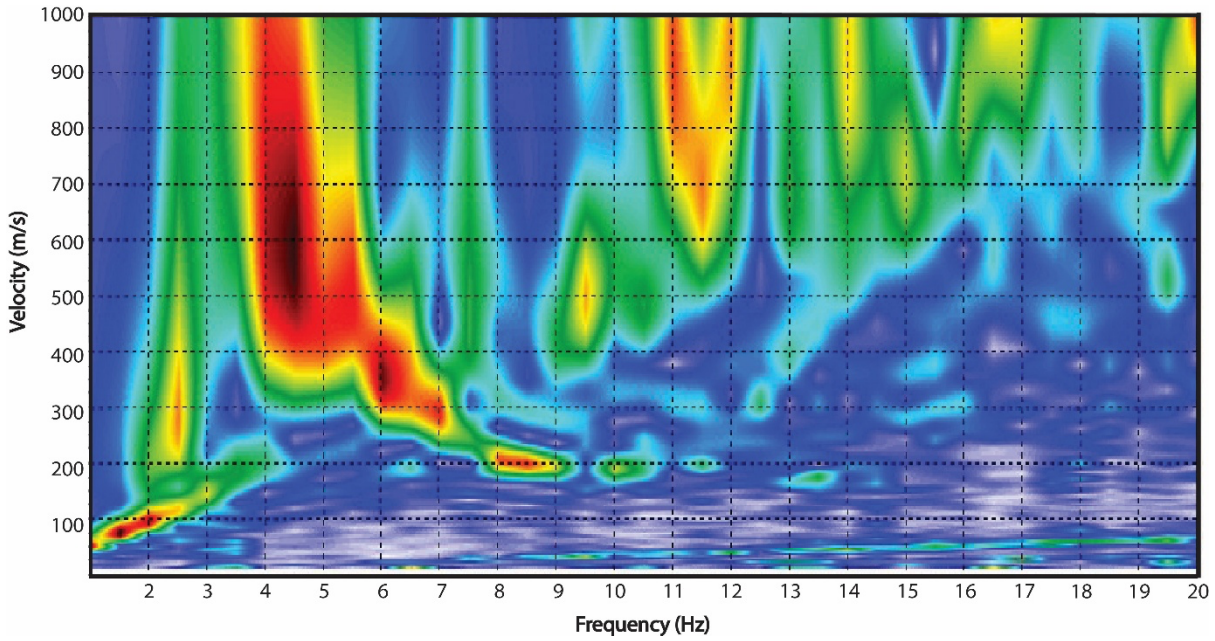

Figure 6. Dispersion pattern with high signal-to-noise ratio of the fundamental-mode Rayleigh wave.

Fundamental mode dispersion curves were picked and inverted to obtain a 2-D section of shear-wave velocity as a function of depth. The apparent velocity (v_{app}) is:

$$v_{app} = \frac{v_{act}}{(\cos\theta)} \tag{1}$$

where v_{act} is the actual seismic velocity and θ is the azimuth of the source with respect to the seismic line determined from the azimuth versus frequency plot. Thus, the percent increase in velocity (Δv) is:

$$\Delta v = \frac{1}{\cos\theta} - 1 \tag{2}$$

Equation 2 was used to calculate the increase in velocity due to the source azimuth for each line (Table 2).

Table 2. Directions of the passive seismic sources and the seismic lines; spread length used for processing, the angle of the source with respect to the line (θ, in degrees counterclockwise from east), and the percent increase in apparent velocity (Δv) attributable to oblique source orientations.

	processing spread length(s)	source orientation	line orientation	θ	Δv
Line 1	90 m 90 m	150° 0°	135° 180°	15° 180°	3.53% 0%
Line 3	99 m	180°	180°	0°	0%
Line 4	81 m	180°	180°	0°	0%
Line 5	99 m	180°	180°	0°	0%
Line 7	99 m	155°	175°	20°	7.0%
Line 8	72 m	180°	180°	0°	0%
Line 9	99 m	90°	86°	4°	0.24%
Line 10	81 m	180°	180°	0°	0%
Line 11	72 m	45°	74°	29°	13.5%
Line 12	81 m	160°	152°	8°	1.00%
Line 13	81 m	160°	172°	12°	2.23%
Line 14	81 m	225°	35°	190°	1.52%
Line 15	81 m	0°	165°	165°	3.40%

Field Results and Observations

General Trends

The average velocity of the upper 15 m is approximately 175 m/s, consistent with the unconsolidated/alluvial sediment in this area and downhole data acquired in well 15B in January 2023. The velocity gradient at 15 m coincides with the interface between the unconsolidated sediment and shale bedrock. Average depth of investigation was 50–60 m across all lines because of surface wave frequencies generally above 4 Hz—lower frequencies would have resulted in deeper sampling depths. Dispersion curves were obtained using varying spread lengths for each line, selected to avoid distortion in surface wave dispersion patterns at low frequencies. Using the shortest optimal spread length on each line resulted in high lateral resolution and the largest spatial extent of the resulting 2-D profiles while maintaining dispersion patterns at lower frequencies.

Line 1

Line 1 (Figure 7) is a slightly curved NW–E oriented line that runs parallel to the V&S railroad and extends across wells 8A, 10B, 11B, 44, 17, 42, 23B, and 41 (Table 3). To optimize source alignment, two different sources were used to process the line: one with an azimuth of 120 degrees and the other 180 degrees.

Table 3. Wells and corresponding station numbers across line 1.

Well	8A	10B	11B	44	17	42	23B	41
Station No.	1033	1086	1105	1136.5	1152.5	1196	1223.5	1265

Line 1 has remained relatively consistent throughout surveys. A halo anomaly at well 8A observed in 2020 persisted relatively unchanged in 2021 and 2023 (Figure 7b). Signal strength

and the presence of higher modes appear to have affected the eastern part of the line past station 1240 in 2015 and 2017. A relatively subtle velocity anomaly east of well 8A was present in multiple surveys. A dome-shaped anomaly was present near stations 1150-1180 (between wells 17 and 42) in 2017, 2018, and again in 2020. In 2023 and 2024, the anomaly near well 8A was not present and velocities are similar to the rest of the line. The velocity variation across line 1 is minimal and identified anomalies are within the bounds of native material properties.

Overall, the bulk-velocity trend observed in April 2025 is generally consistent with results from the past three years (Figure 7d). The maximum depth of investigation was between 45 and 65 m, which is deeper than the 2024 survey. The area surrounding well 8A has slightly elevated velocity, similar to prior surveys. Velocity variation across line 1 is minimal and within the bounds of native material properties and a normal stress regime.

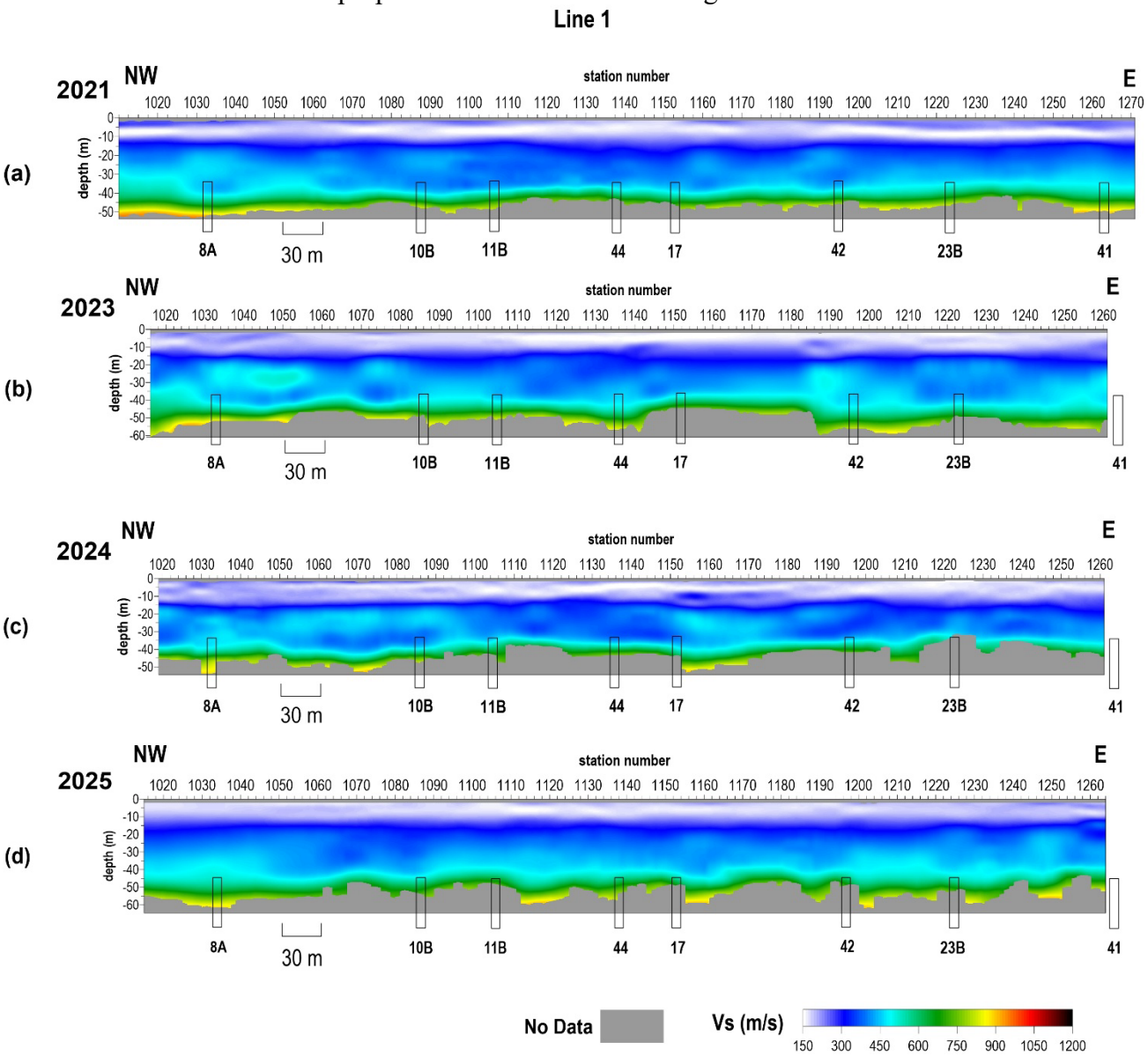

Figure 7. Shear wave velocity profiles from line 1 from (a) November 2021, (b) March 2023, (c) August 2024, and (d) April 2025.

Line 3

Line 3 (Figure 8) is oriented W–E just north of Carey Boulevard and extends over wells 46, 45, 22A, 23, 29, 30, 39, and 92 (Table 4).

Table 4. Wells and corresponding station numbers across line 3.

Well	46	45	22A	23	29	30	39	92
Station No.	3025	3057	3080.5	3124	3148	3183.5	3199	3230.5

Line 3 has remained largely consistent throughout surveys with the bulk velocity trends, with localized anomalies at a few wells. Weaker fundamental modes were observed at the west end of the line in 2018 and 2019, spanning stations range 3015-3035 and 3053-3075. A halo anomaly was observed just outside this range from stations 3072-3082, just west of well 22A, in 2018 and 2020. A subtle dome-shaped anomaly was observed in proximity to well 22A in 2024. The velocity profiles near well 23 (stations 3215-3240) are somewhat variable from year to year and may be associated with redistribution of stress in the overburden due to localized failure. In 2024, velocity was consistent across the line, consistent with native material properties and a normal stress regime.

Overall, the 2025 results remain similar to 2024 and within the range expected for native bedrock (Figure 8d).

Line 4

Line 4 is a W–E oriented line that intersects wells 90, 89, 88, and 87 at stations 4044, 4076, 4107.5, and 4139.5, respectively (Figure 9). This line is located south of the closed section of Carey Boulevard with the east end of the line terminating west of Fairlawn Cemetery.

In 2017, depths of investigation were limited due to poor signal below 5.5 Hz. In 2018, fundamental energy was less coherent from stations 4120-4130 due to a higher mode and monitoring was recommended due to a decrease in velocity between wells 90 and 89. In 2019, source signal was coherent with good S/N throughout the line, and no velocity anomalies were observed. In 2020, anomalous bedrock velocity was observed between stations 4050 and 4055. In 2024, an area of slightly increased depth of investigation was observed between wells 87 and 88. Velocities between these wells were elevated at low frequencies, contributing to longer wavelengths and, thus, increased depth of investigation. Due to low S/N in this area, it was unclear whether the apparent velocity increase is due to a true increase or a result of interference from higher mode surface wave energy. This anomalous feature was consistent using multiple passive sources and, therefore, warranted attention and additional scrutiny in future annual monitoring surveys.

In 2025, a window splitting algorithm was used to enhance the S/N of passive source amplitudes, providing strong fundamental mode signal. The area of elevated velocities observed between wells 87 and 88 in 2024 is not present in 2025 (Figure 9d), supporting that the anomalous characteristics observed in 2014 were likely a result of low S/N or interference. Bulk velocities are consistent across the line and like previous years, representing native properties.

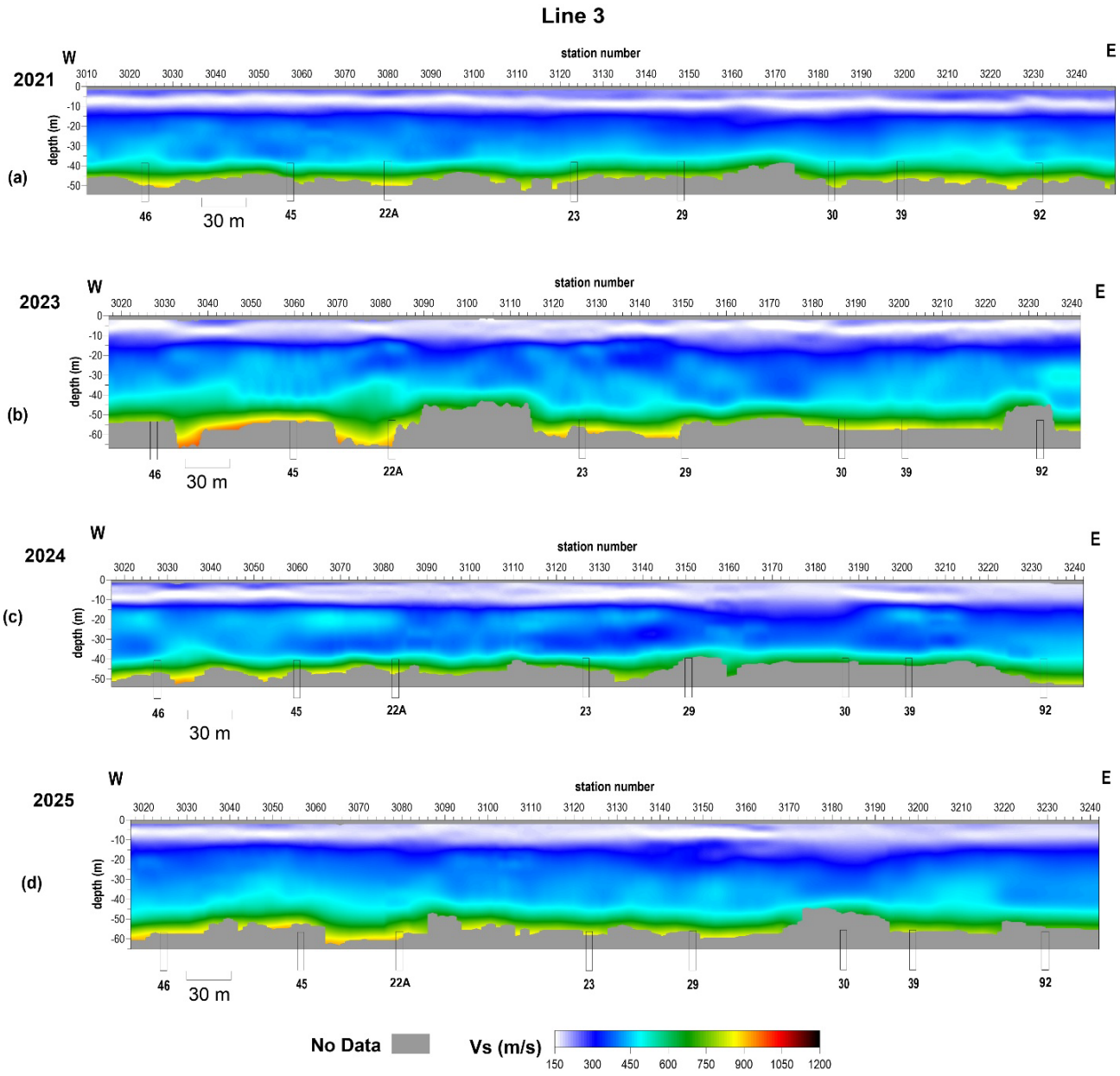

Figure 8. Shear-wave velocity profiles from line 3 from (a) November 2021, (b) March 2023, (c) August 2024, and (d) April 2025.

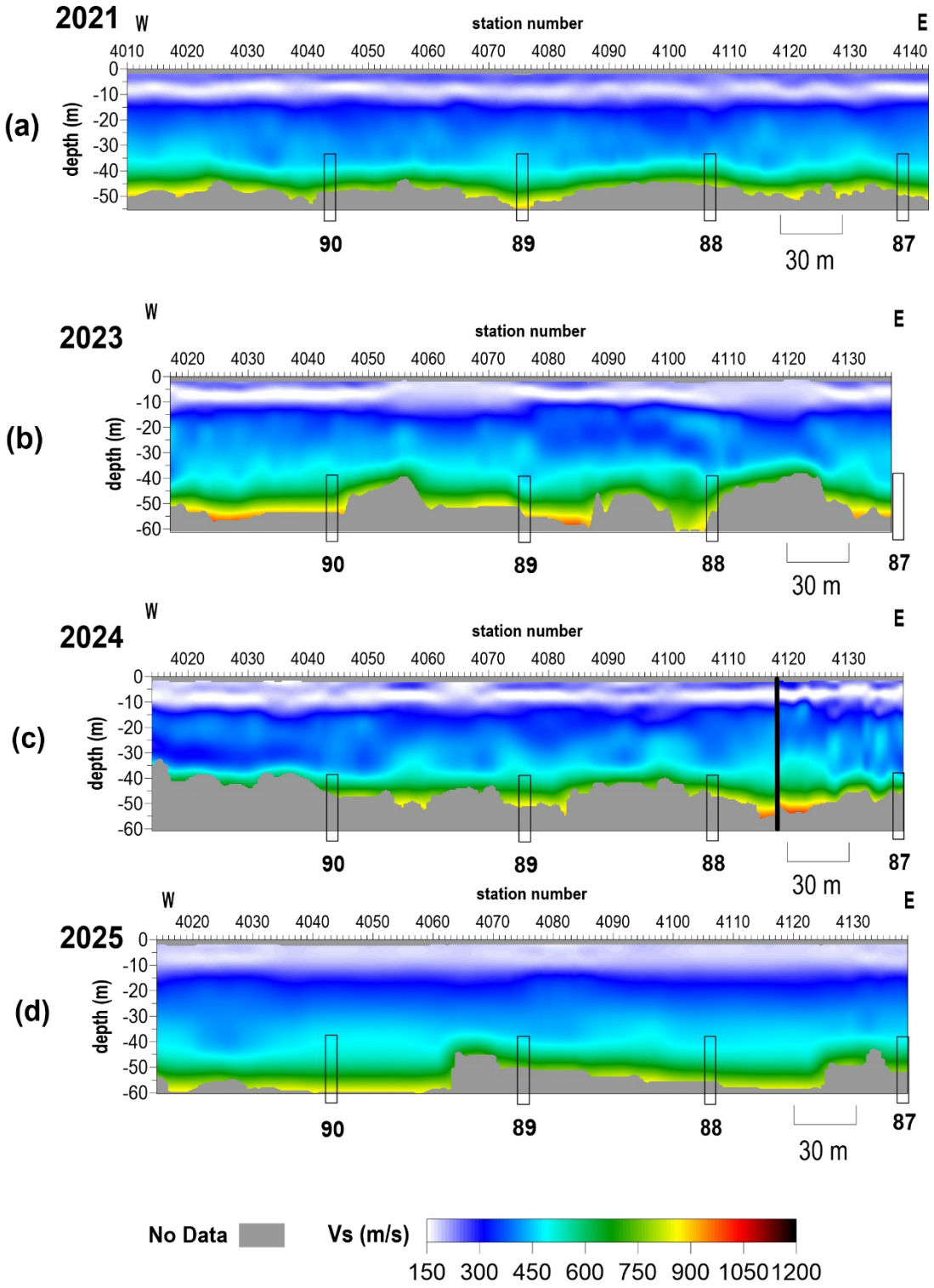

Figure 9. Shear-wave velocity profiles from line 4 from (a) November 2021, (b) March 2023, (c) August 2024, and (d) April 2025.

Line 5

Line 5 is oriented W–E and extends over wells 4B, 2B, 12B, and 14B at stations 5027.5, 5061, 5094, and 5126.5, respectively (Figure 10). This line is located just south of the Irsik and Doll grain elevators with the west end of the line crossing the paved entry road north of Carey Boulevard.

Line 5 has been variable with multiple velocity anomalies observed in past surveys. Velocity on the west half of the line was elevated over wells 4B and 2B in 2017. In 2019 and 2020, a dome-shaped area of elevated velocity was observed near well 4B. Reprocessing of this data indicated variable signal quality and changes in the depths of investigation near well 4B, which could suggest dynamic processes at depth. Multiple fundamental modes have historically been observed near well 4B and between wells 2B and 12B, which could account for these anomalies and possibly suggest heterogeneity at depth. In 2021 and 2023, an area of elevated velocity was observed west of well 14B, warranting attention. However, velocity at well 14B returned to normal in 2023.

Overall, the velocity profile in 2025 is consistent with native properties (Figure 10d). An area of slightly elevated velocity near well 12B at a depth of about 40 m is likely a result of variability due to uncertainty in the low frequency portion of the fundamental mode in this area.

Line 7

Line 7 is oriented WNW–ESE and extends over wells 8B, 15B, and 18 at approximately stations 7028, 7073, and 7114, respectively (Figure 11). This line is located between the V&S and BNSF railroads.

Well 15B has a history of dynamic shear-wave velocity and depth of investigation (see Figure A-1 in the appendix). An area of slightly elevated velocity and deeper depth of investigation was observed centered on well 15B in 2015, possibly suggested longer wavelengths and, thus, elevated velocity at depth. Reprocessing focused on the upper 50–60 m suggested no elevated velocity within this depth range. Increased depth of investigation and longer wavelengths were again observed in 2018 and 2020. Velocities returned to normal and consistent with the rest of line 7 in the December 2020 survey. In 2023, a dome-shaped area of elevated velocity was observed west of well 18 (Figure 11b). However, this area was likely due to higher mode interference in the dispersion curves and was not present in the 2024 survey.

Results of the 2025 survey are similar to 2024, with slightly lower frequency and, thus, deeper depth of investigation on the east end of the line (Figure 11d). Overall bulk velocity is similar to previous surveys and is consistent with native material properties.

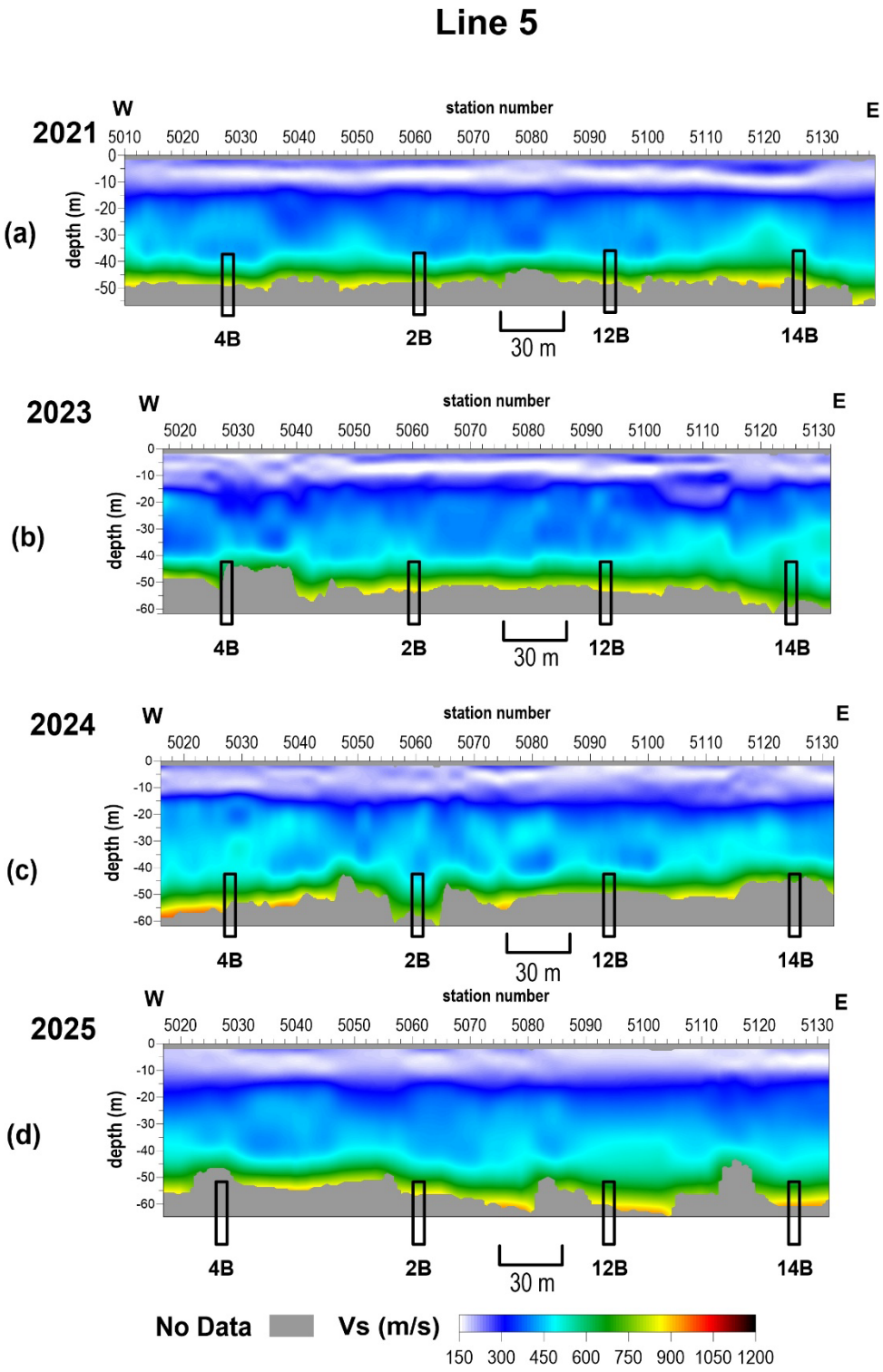

Figure 10. Shear-wave velocity profiles from line 5 from (a) November 2021, (b) March 2023, (c) August 2024, and (d) April 2025.

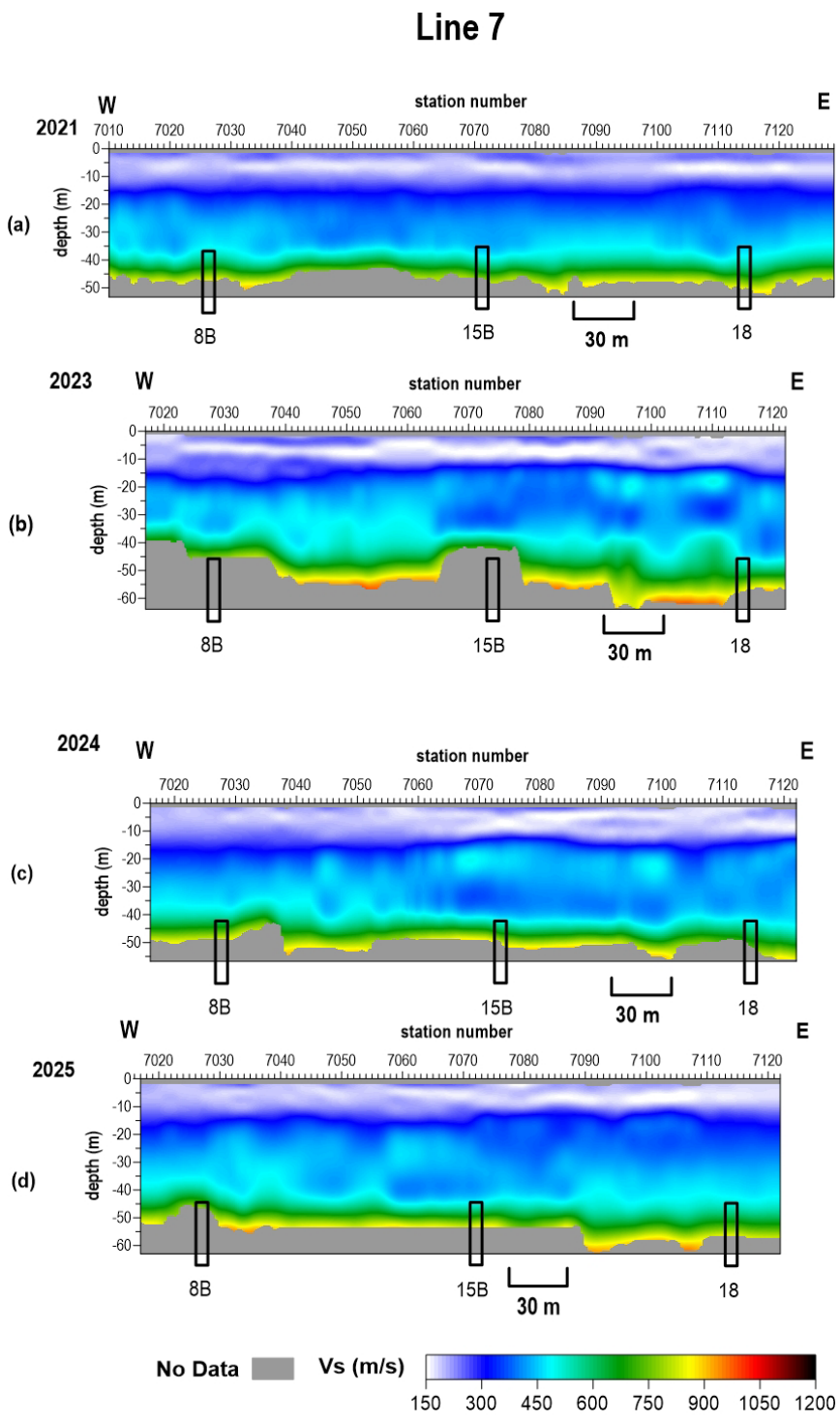

Figure 81. Shear-wave velocity profiles from line 7 from (a) November 2021, (b) March 2023, (c) August 2024, and (d) April 2025.

Line 8

Line 8 is oriented W–E and intersects well 13B at station 8025 (Figure 12). The westernmost four stations on line 8 (8008-8011) extend across the paved entry road north of Carey Boulevard; these four stations required rock plates rather than steel spikes to couple sensors to the ground surface.

Only subtle velocity changes have been observed at well 13B in the past few years. Velocity was slightly elevated in 2017 and returned to normal stress conditions representative of native areas in 2018. A minor velocity inversion was observed in 2020, but conditions returned to levels considered normal since 2021. Bedrock velocity was slightly elevated in 2024 but within the expected normal range for this site. While these timelapse observations may reflect periodic stress build up, roof failure, and associated drops in stress, the subtle changes are more likely a result of inherent uncertainty in the method.

Bulk velocity in 2025 decreased relative to 2024, representing a return to native properties/conditions and likely suggests current stability (Figure 12d).

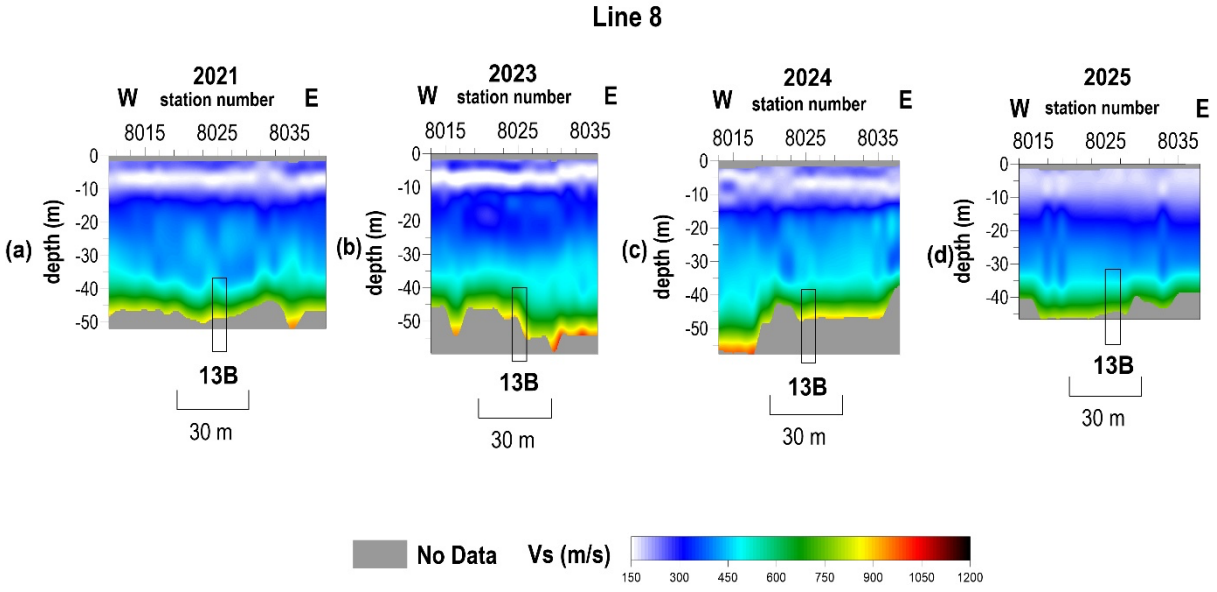

Figure 92. Shear-wave velocity profiles from line 8 from (a) November 2021, (b) March 2023, (c) August 204, and (d) April 2025.

Line 9

Line 9 is oriented N–S parallel to William Street and intersects wells 52, 53, 59, and 60 at stations 9031, 9061, 9098, and 9127, respectively (Figure 13).

Velocities in the upper 30 m of line 9 are generally consistent, but bedrock velocity has been variable below 30 m. Velocity across the line was elevated in 2018 and remained elevated between wells 53 and 59 in 2018. Velocity trends below 30 m have varied slightly over time and have typically been elevated compared to other lines at this site. In 2023, velocities below 30 m were elevated on the northern half of the line (spanning wells 52 and 53) compared to the southern half (spanning wells 59 and 60). In 2024, velocities on the northern half of the line decreased and are consistent with the south half of the line. These observations may suggest dynamic processes at depth (possibly localized failure and redistribution of stress at wells 52 and

53, possibly suggestive of the presence of a gallery—especially considering the static nature of the most resent sonar in well 53.

The overall Vs trend in 2025 is similar to 2023, with slightly elevated velocities at the north end of the line between wells 52 and 53, indicating continued dynamic conditions (Figure 13d). Velocities at the southern half of the line near wells 59 and 60 have remained relatively consistent over the past three years, suggesting relative stability. Variability in the depth of investigation in 2025 is a result of interference from offline source energy and/or higher mode surface waves.

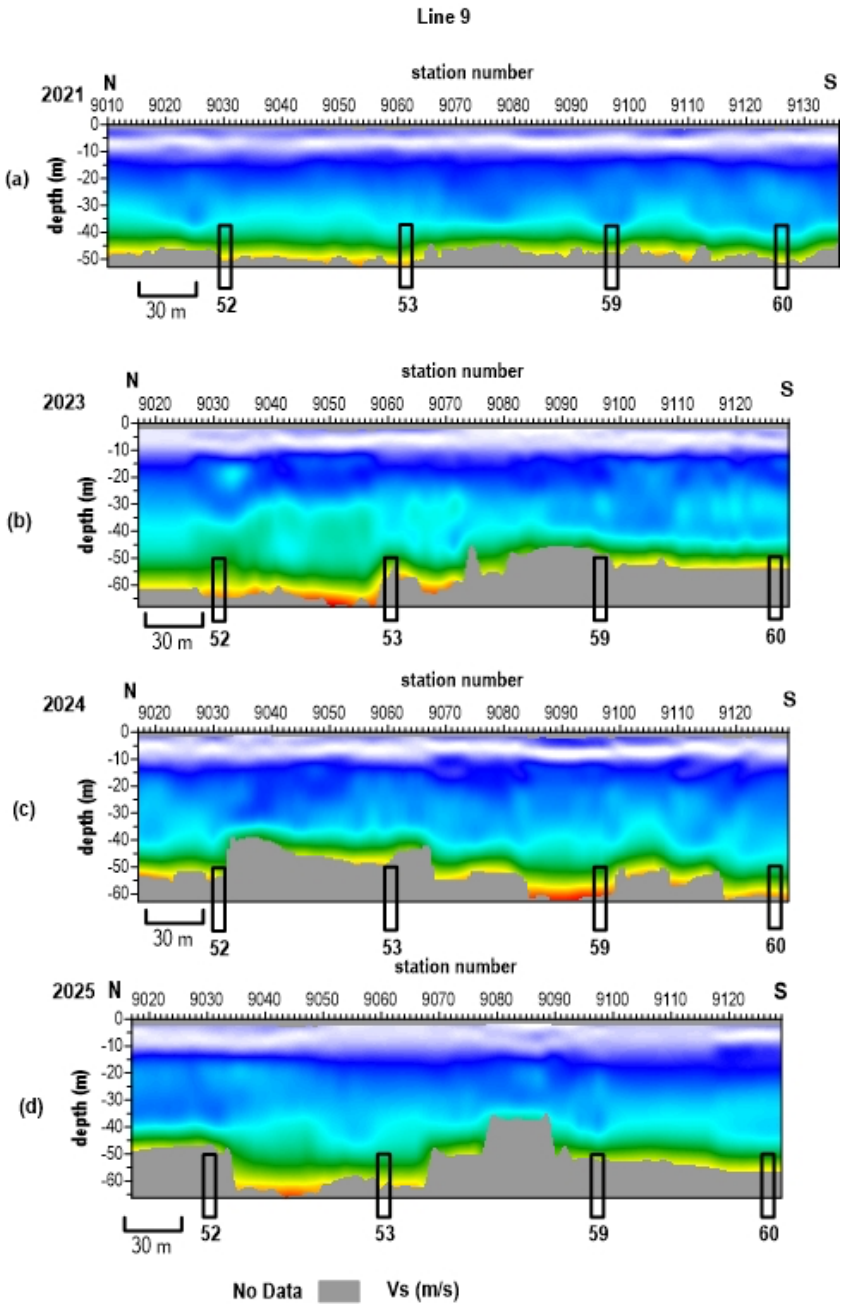

Figure 103. Shear-wave velocity profiles from line 9 from (a) November 2021, (b) March 2023, (c) August 2024, and (d) April 2025.

Line 10

Line 10 is a W–E oriented line that intersects well 2A at station 1022.5 (Figure 14). Line 10 is located just north of the Irsik and Doll grain elevators parallel to the elevator access road.

Timelapse changes observed at well 2A since 2013 suggest periods of elevated stress/velocity, subsequent roof rock failure and reduced overburden strength, and periods of relative stability (see Figure A-2 in the appendix). Between the 2015 and 2017 surveys, velocity in the overburden at well 2A increased slightly (~15%) and was consistent with native bedrock velocity. This suggests the void at that time was in a state of relative stability with only gradual changes in stress. Multi-mode behavior was noted west of well 2A in 2020 suggesting heterogeneity at deeper depths where multiple stress states may have existed within the shale bedrock, and a period of relative stability in 2021. Velocity was slightly elevated in 2023 and increased 30% or more in 2024 relative to the expected velocity for native conditions.

The velocity on line 10 has decreased compared to 2024, and largely represents velocities expected for native properties/conditions at this site (Figure 14d).

Line 11

Line 11 is oriented N–S and intersects well 2A at station 1124 and well 4B at station 1151 (Figure 15). Well 5B is in proximity to the southern end of the line. Line 11 extends through the Irsik and Doll grain elevators and intersects line 10 on the northern end of the line.

In general, the velocity profile below 30 m has been lower on line 11 than on the nearly perpendicular line 10. The velocity variation is azimuthal and therefore anisotropic, which may be associated with changes in material strength associated with fractures. In 2023 and 2024, velocities are similar to 2020, possibly suggesting azimuthal anisotropy and changes in material strength influenced by fracture orientation. This anisotropy is particularly apparent in 2024, given the relatively large increase in velocity on line 10.

In 2025, velocity on line 11 remains similar to the previous few years (Figure 15d). Due to the velocity decrease and return to expected velocities on line 10, velocities on lines 10 and 11 were not anisotropic at the time of the 2025 survey.

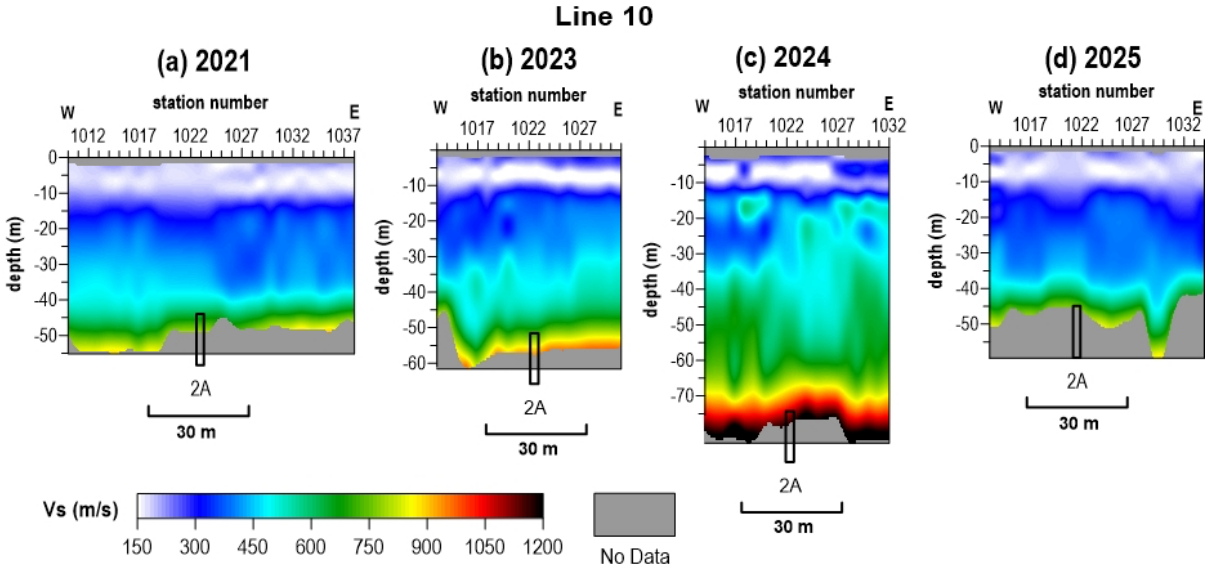

Figure 14. Shear-wave velocity profiles from line 10 from (a) November 2021, (b) March 2023, (c) August 2024, and (d) April 2025.

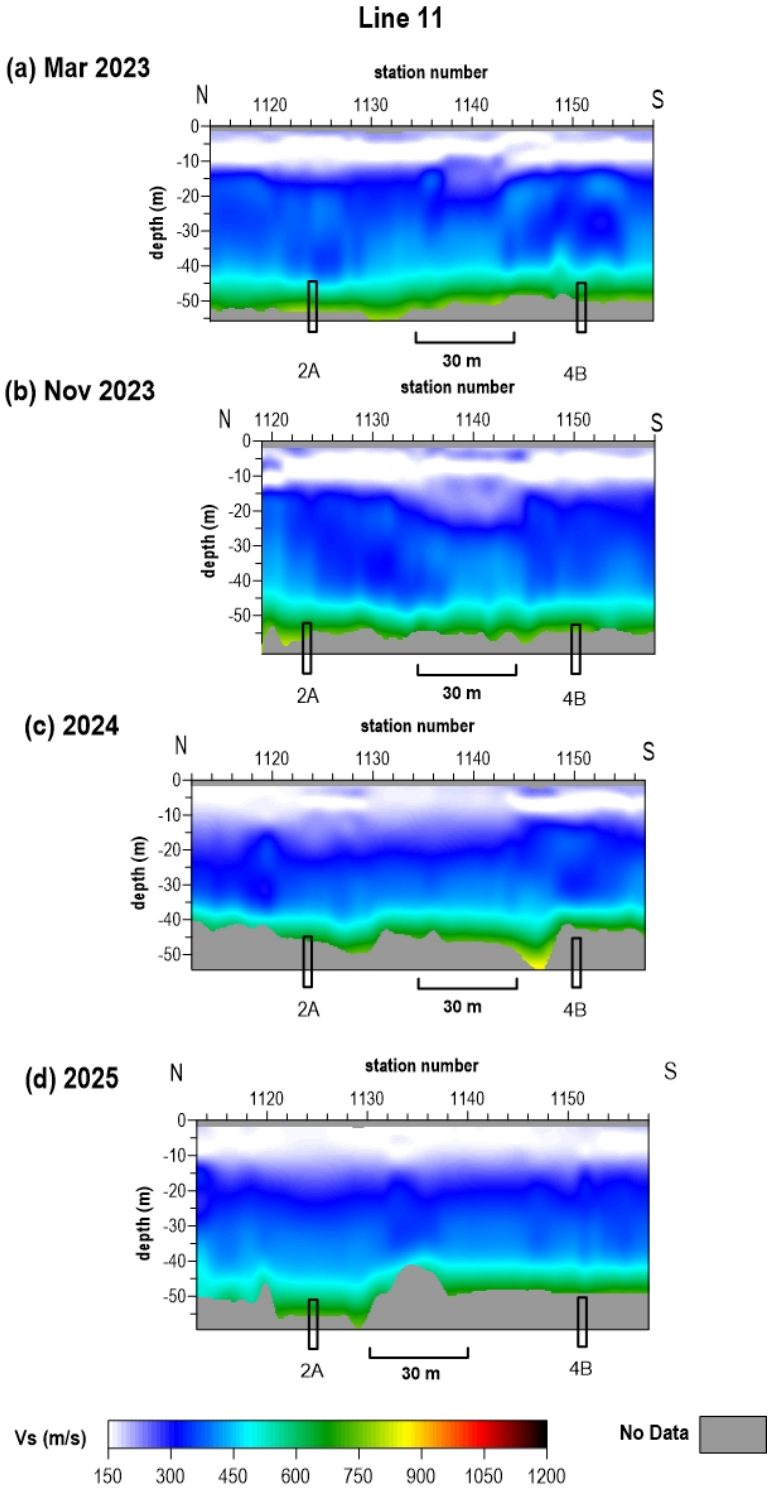

Figure 15. Shear-wave velocity profiles from line 11 from (a) November 2021, (b) March 2023, (c) August 2024, and (d) April 2025 investigation with approximate locations of well 2A and well 4B.

Line 12

Line 12 is a NW–SE oriented line that intersects wells 6B and 7B at stations 1238 and 1219, respectively (Figure 16). The west end of the line is south of the Irsik and Doll grain elevators and the east end of the line is just north of Carey Boulevard.

The velocity on line 12 was static through 2020. Velocities were slightly elevated in 2021 compared to previous years but still within the range of bedrock velocity estimates on other lines at the CBRA and may have been a result of higher mode interference with the fundamental mode. In 2023, a subtle dome-shaped area of elevated velocity was observed in proximity to well 7B. These velocities were still within the expected range for bedrock at this site but may suggest gradually elevating velocity and possibly the start of increasing stress at 7B. It is possible the apparent velocity is higher due to uncertainty in dispersion curve picks from reduced S/N at corresponding frequencies. The 2024 passive sources were very challenging to pick due to interference of higher mode or off-line energy, despite processing designed to enhance fundamental mode signal. Because of inversion instability, results from the 2024 survey were artifact-rich and uninterpretable.

The 2025 survey had records with stronger signal, resulting in a more stable inversion. Velocity is slightly elevated below 30 m across the line (Figure 16d). Given the relative stability of velocities the several few years, it is likely not a cause for concern currently and does not require a mid-year monitoring survey. However, given the inversion instability in 2024, apparently elevated velocity in 2025 warrants heightened awareness.

Line 13

Line 13 is oriented WNW–ESE and intersects wells 7A and 4A located approximately at stations 1328 and 1376.5, respectively (Figure 17). This line is located south of the BNSF railroad at the northwest corner of the site.

Bulk velocity on line 13 has remained relatively static since monitoring began on this line in 2017. An apparent increase in velocity between 7A and 4A was observed in 2023 was interpreted as a result of uncertainty. The velocities returned to native conditions in 2024, supporting the initial interpretation.

Velocities in 2025 are similar to, although slightly lower than 2024 (Figure 17d). Velocity values across this area are within normal range for native material and represent a normal stress regime. Velocity variability on this line is largely a result of uncertainty inherent to the MASW method.

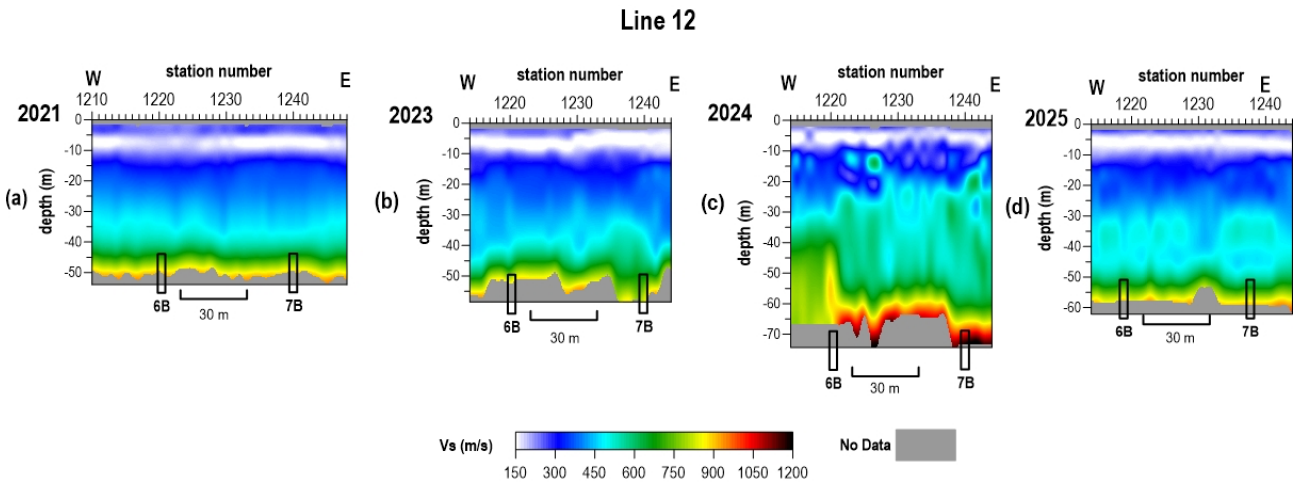

Figure 16. Shear-wave velocity profiles from line 12 from (a) November 2021, (b) March 2023, (c) August 2024, and (d) April 2025 investigation.

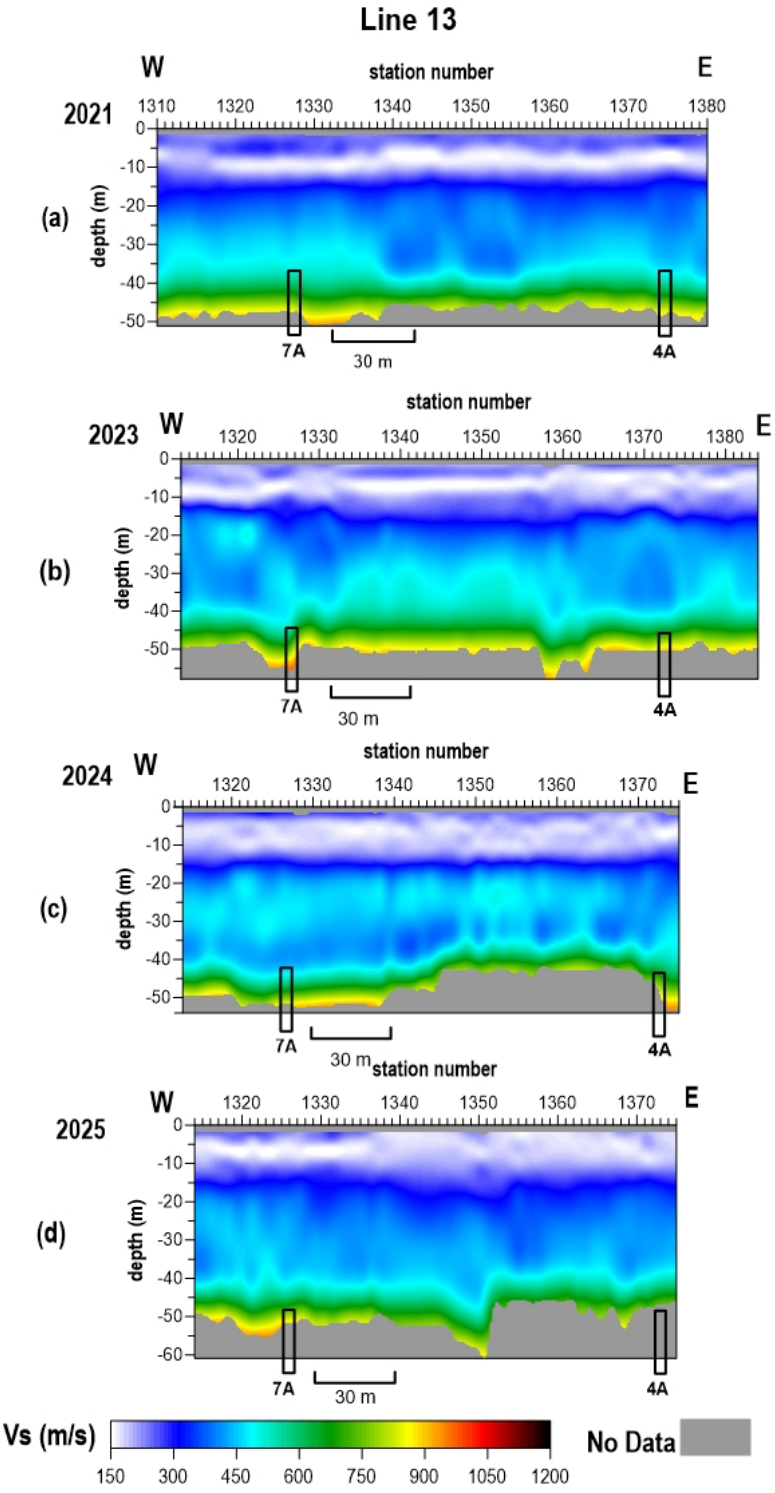

Figure 17. Shear-wave velocity profiles from line 13 from (a) November 2021, (b) March 2023, (c) August 2024, and (d) April 2025 investigation.

Line 14

Line 14 is oriented SW–NE and extends across wells 3B and 1B, located at stations 1430 and 1450, respectively (Figure 18). The southwest end of line 13 is located south of the Irsik and Doll grain elevators and the northeast end of the line is located north of the V&S railroad.

Line 14 has remained static historically with only minor velocity variability. In 2018, the velocities were reported to be 14% higher than in 2017. However, it was determined that offline source energy was used in 2018 resulting in an apparent not true increase in velocity. The velocity profile in 2019 was consistent with the 2017 survey. In 2021, slightly elevated velocities were observed west of well 3B but within the expected bedrock velocity range. Higher mode surface waves were observed in that area in past surveys, and the apparent elevated velocity is likely a result of higher mode interference.

Greater depths of investigation were achieved in 2025 due to stronger signals at lower frequencies (Figure 18d). There is an area of increased velocity across the west end of the line centered on well 3B. The S/N of the fundamental mode on this line is lower than previous years. Therefore, the apparent increase in velocity on the west of the line may be due to uncertainty.

Line 15

Line 15 is orientated WNW–ESE over wells 19, 20, 25, 26, 33, 36, and 94 (Table 5) and is located just south of the BNSF railroad. This line was a new addition to the passive monitoring survey in 2021 and spans a portion of a 2-D profile recorded during a 2010 passive surface wave survey.

The overall bulk velocity trend in 2023 was largely consistent with the 2021 and 2010 surveys with only subtle (~15%) variability (Figures 19 and 20). Considering the plugged status of the wells along the railroad tracks, the velocity profile and apparent variability year-to-year between wells 25 and 94 represents normal variability in the estimated shear velocity.

The velocity profile in 2025 (Figure 19d) is consistent with the previous studies along this line and represents native material properties and a normal stress regime.

Table 5. Wells and corresponding station numbers across line 15.

Well	19	20	25	26	33	36	94
Station No.	15025	15058	15080	15123	15138	15174	15207

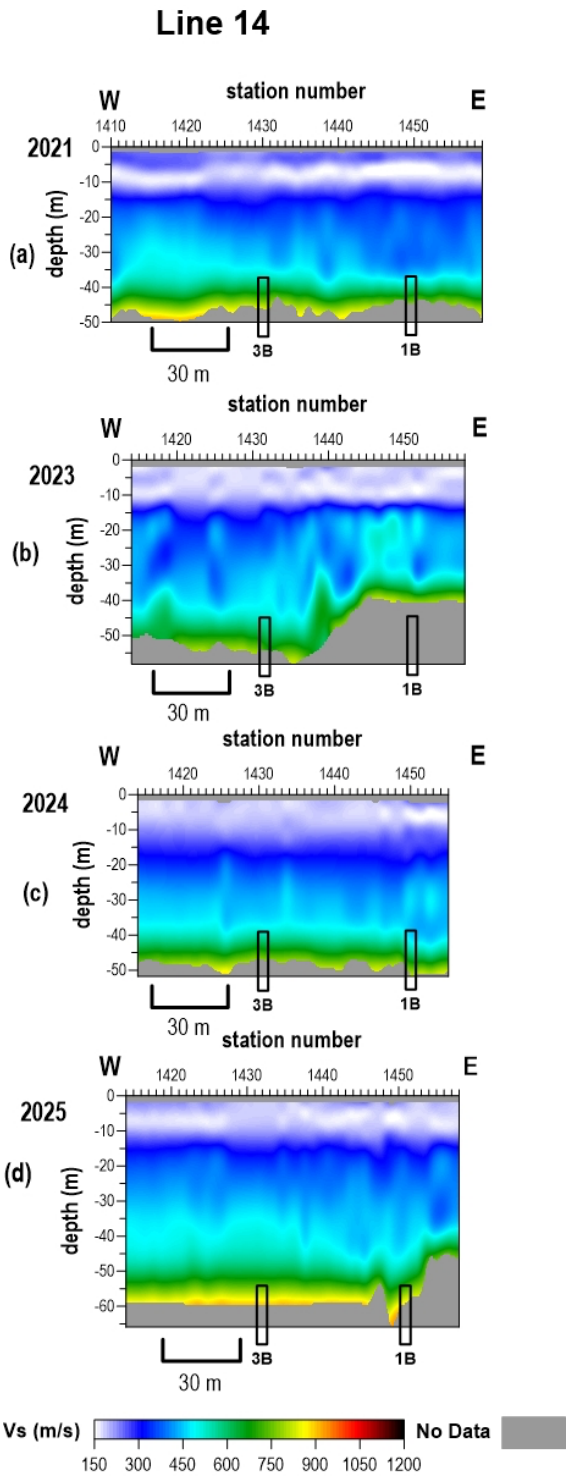

Figure 18. Shear-wave velocity profiles from line 14 from (a) November 2021, (b) March 2023, (c) August 2024, and (d) April 2025 survey.

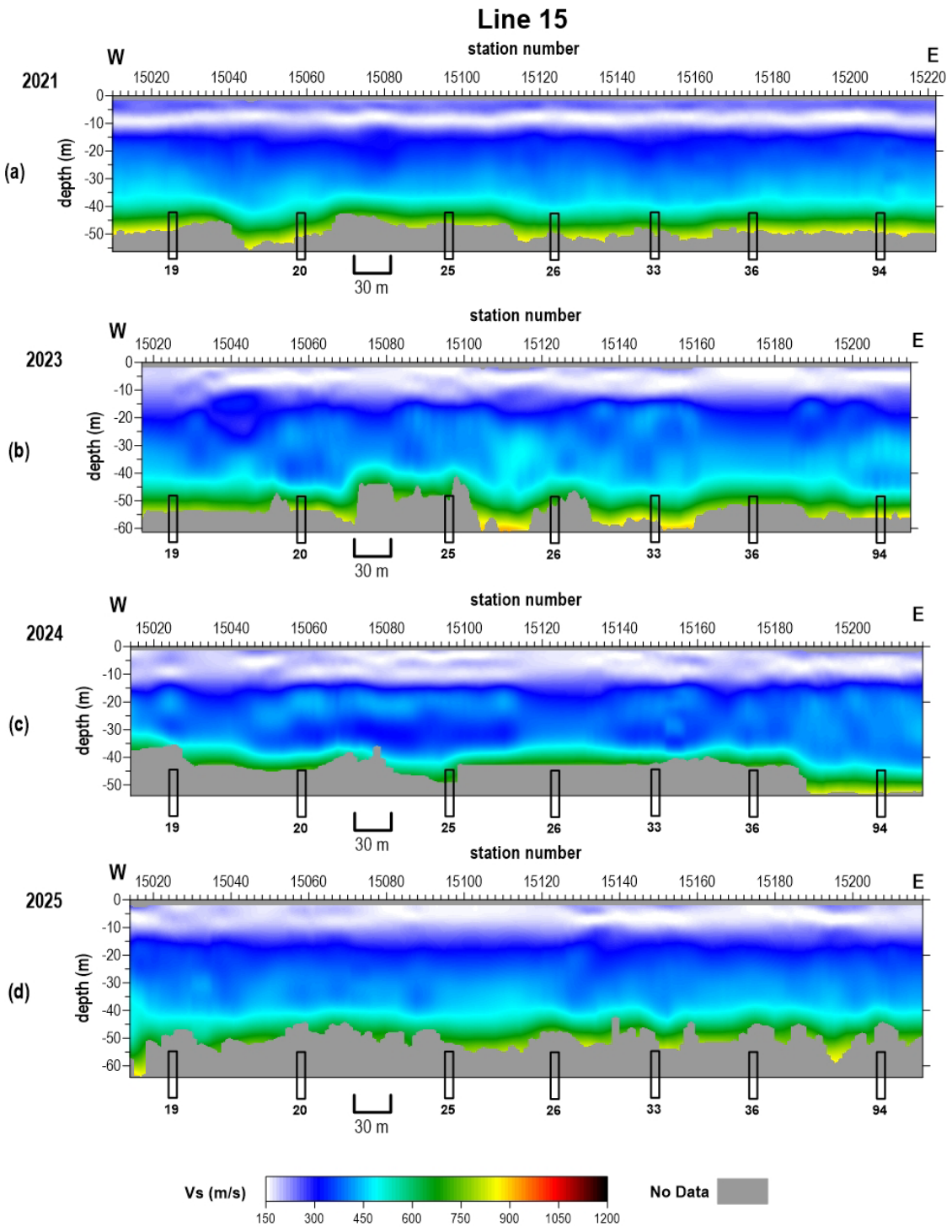

Figure 19. Shear-wave velocity profile from line 15 from (a) November 2021, (b) March 2023, (c) August 2024, and April 2025.

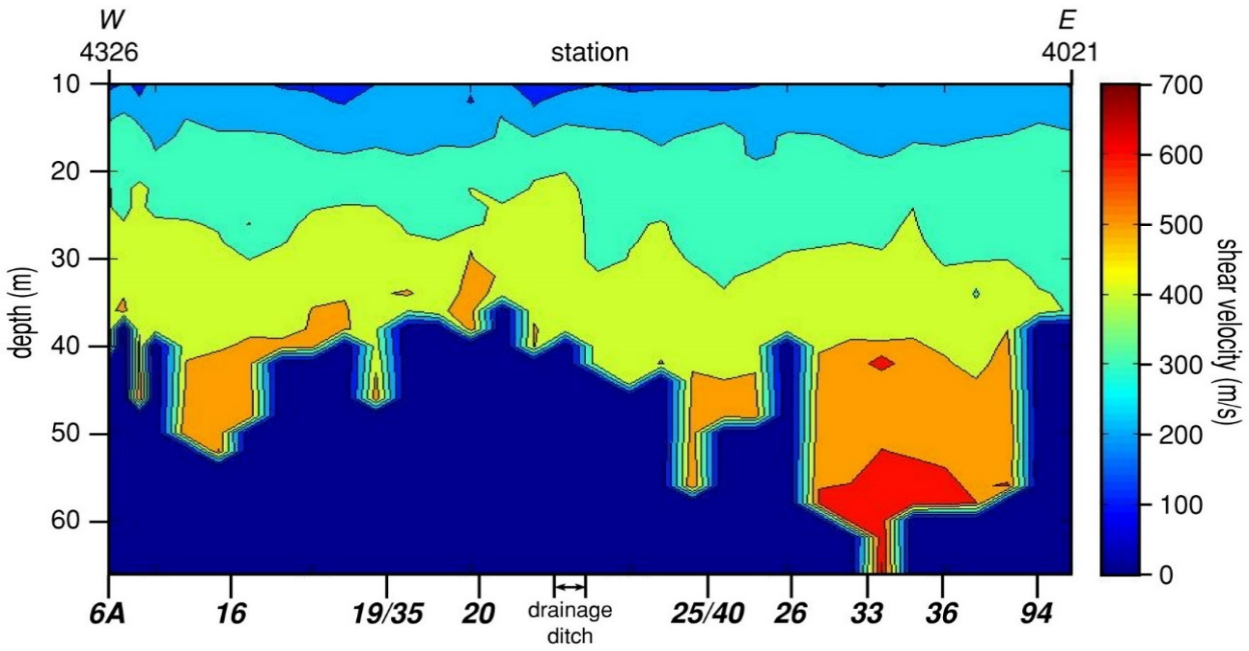

Figure 20. Shear wave velocity profile from the 2010 survey over the location of line 15 in the current survey.

Conclusions

Overburden materials at or near seven wells from this April 2025 survey were interpreted to have subtle but notable changes in overburden characteristics relative to past years or native material properties. Bedrock velocity at well 2A, a major focus of past reports due to dynamic overburden conditions and possible limited failure at depth, experienced a 30% reduction in velocity along line 10, suggesting dynamic changes continue in this area. Timelapse variability may suggest dynamic stress changes associated with changes in roof structures or characteristics of salt jugs have occurred near wells 3B, 6B, 7B, 8A, 52, and 53. Apparent shear-wave velocity at these wells is slightly elevated compared to previous surveys, possibly representing increased stress at depth but likely related to surface wave propagation characteristics (e.g., higher mode interference) or reduced S/N. The relatively small velocity increases do not appear to suggest an imminent threat of vertical migration at this time.

Based on nearly a decade of passive seismic monitoring at most of the 47 wells sampled in this survey, shear-wave velocity profiles are classified into three different categories: (1) wells with normal or currently stable stress regime (little to no recent timelapse variability), (2) wells with recent timelapse variability, but interpreted as currently normal/stable stress regime, or (3) wells with recent timelapse variability and possibly elevated stress.

Wells interpreted with normal or currently stable stress regime (little to no recent timelapse variability)

Wells 1B, 2B, 3B*, 4A, 5B, 6B*, 7A, 7B*, 8A*, 8B, 10B, 11B, 12B, 13B, 15B, 17, 18, 19, 20, 23, 23B, 25, 26, 29, 30, 33, 36, 39, 41, 42, 44, 45, 46, 59, 60, 87, 88, 89, 90, 92, and 94.

* Given the historically minimal timelapse variability on this line, conditions at these wells are likely stable but observations from 2024-2025 justify heightened awareness and additional scrutiny in future monitoring surveys.

Wells with recent timelapse variability, but interpreted as currently normal/stable stress regime

Well 14B (line 5)

A dome-shaped area of elevated velocity appeared west of well 14B in 2021. Although velocity returned to normal at this location in 2023, the velocity at well 14B was slightly elevated with a subtle velocity halo east of well 14B. Timelapse observations at this well over the past few years suggest dynamic stress changes have occurred that could be associated with changes in the roof structures/characteristics of the salt jug. In 2024 and 2025, the velocity profile at this well is consistent with the rest of this line, suggesting redistribution of stress and relative stability.

Well 22A (line 3)

An area of elevated velocity was observed between wells 17 and 42 (line 1) and 45 and 22A (line 3) in 2020. In 2021 and 2023, the overall velocity trend was more consistent with 2019, with a more uniform profile between wells on lines 1 and 3 with only subtle velocity hallows near wells 17 and 42. A 30 m dome-shaped area of elevated velocity observed near well 22A was observed in 2023 and is worth monitoring in future surveys. In general, these observations are consistent with the dynamics these wells have demonstrated in years past and the absence of an anomaly at well 22A in 2024 and 2025 suggests relative stability at the time of the survey. This level of stress variability is likely characteristic of some jugs due to geometry, depth, or volume. As long as the stress field above the dolomite at 70 m periodically returns to a more "normal" state with no apparent structural abnormality, then the observed dynamics are likely associated with strain at jug depths and not dramatically affecting the bulk strength of the overburden.

Wells 87 and 88 (line 4)

An area of slightly increased depth of investigation was observed between wells 87 and 88 in 2024. Velocities between these wells are elevated at low frequencies, contributing to longer wavelengths and, thus, increased depth of investigation. Due to low signal-to-noise in this area, it was unclear whether the apparent velocity increase was due to a true increase or a result of interference from higher mode surface wave energy. This anomalous feature was consistent using multiple passive sources and, therefore, warrants attention and additional scrutiny in future annual monitoring surveys. Given the return to normal Vs in 2025, the apparent velocity increase was likely a result of interference. Absence of this anomaly in future surveys will strengthen this interpretation.

Wells with recent timelapse variability and possibly elevated stress

Wells 2A and 4B (lines 10 and 11)

Elevated Vs and timelapse changes have been observed along lines 10 and 11, most notably at well 2A. Multi-mode surface wave dispersion patterns are potentially indicative of heterogeneities below the imaging depth of these data. Azimuthal variation

in bedrock velocity (anisotropy) between lines 10 and 11 has been persistently observed since 2018. These timelapse changes and velocity anisotropy on lines 10 and 11 suggest the possibility of dynamic stress changes. It is not clear from these data how much strain can be suggested to have occurred beyond the elastic/plastic boundary from these stress observations alone.

A lack of timelapse changes in VSP data acquired in well 2A (Peterie et al., 2025) is evidence that no significant vertical migration occurred between downhole surveys in 2023 and 2024, despite a notable increase in Vs along line 10 observed in the 2024 passive wave survey. Therefore, elevated Vs observed in the passive seismic was likely caused by changes in Young's Modulus due to increased stress but either (1) not yet at a level sufficient for macro strain (failure) instigating vertical migration of the roof, or (2) the strain resulted in failure and has been actualized through increases in the horizontal expanse of the cavern roof without measurable vertical change. Reduced Vs in 2025 suggests strain through one of these mechanisms has occurred. Pending results from the VSP acquired at the time of the 2025 passive MASW survey may help determine whether vertical or horizontal failure occurred.

Wells 52, 53 (line 9, William Street)

The velocity gradient in the upper 30 m of the William Street line (line 9) has been reasonably consistent since the beginning of timelapse passive surface wave monitoring. Velocity trends below 30 m have varied slightly over time and have typically been elevated compared to other lines at this site. In 2023, velocities below 30 m were elevated on the northern half of the line (spanning wells 52 and 53) compared to the southern half (spanning wells 59 and 60). In 2024, velocities on the northern half of the line decreased and are consistent with the south half of the line. These observations may suggest dynamic processes at depth (possibly localized failure and redistribution of stress at wells 52 and 53, possibly suggestive of the presence of a gallery—especially considering the static nature of the most recent sonar in well 53. Currently, the velocity profile at line 9 is largely consistent with elsewhere at this site, likely indicative of a current period of relative stability. An area of elevated velocity on the northern portion of the lines suggests stress may be slightly elevated between wells 52 and 53.

Recommendations

The shear-wave velocity directly over or in proximity to the majority of wells in this 2025 study continues to represent natural geologic conditions and a normal stress regime. Based on nearly a decade of passive seismic monitoring at most of these wells, shear-wave velocity profiles are classified into three different categories: (1) wells with normal or currently stable stress regime (little to no recent timelapse variability), (2) wells with recent timelapse variability, but interpreted as currently normal/stable stress regime, or (3) wells with recent timelapse variability and possibly elevated stress. Anomalous shear-wave velocity profiles from seven wells justify an elevated awareness and focused monitoring on future surveys.

Strength characteristics estimated from shear-wave velocities derived from the passive MASW surveys around wells 2A (line 10); 8A (line 1); 6B and 7B (line 12); 3B (line 14); and 52 and 53 (line 9 along William Street) have changed from historical surveys and are suggestive of

possible increases and/or changes in stress due to unstable spans of roof rock above voids. Voids associated with these eight wells currently represent the only apparent potential for void migration toward the ground surface and thereby affecting the stability of material above the bedrock surface in the survey area. In general, with current conditions largely reflecting normal or stable stress regimes with only a few areas possessing subtle and relatively minimally elevated stress, continued monitoring is recommended on an annual basis.

References

Dellwig, L.F., 1963, Environment and mechanics of deposition of the Permian Hutchinson Salt Member of the Wellington shale: Symposium on Salt, Northern Ohio Geological Society, p. 74-85.

Dvorkin, J., A. Nur, and C. Chaika, 1996, Stress sensitivity of sandstones: *Geophysics*, v. 61, p. 444-455.

Eberhart-Phillips, D., D.-H. Han, and M.D. Zoback, 1989, Empirical relationships among seismic velocity, effective pressure, porosity, and clay content in sandstone: *Geophysics*, v. 54, p. 82-89.

Holdoway, K.A., 1978, Deposition of evaporites and red beds of the Nippewalla Group, Permian, western Kansas: Kansas Geological Survey Bulletin 215.

Ivanov, J., R.D. Miller, S.L. Peterie, J.T. Schwenk, J.J. Nolan, B. Bennett, B. Wedel, J. Anderson, J. Chandler, and S. Green, 2013, Enhanced passive seismic characterization of high priority salt jugs in Hutchinson, Kansas: Preliminary report to Burns & McDonnell Engineering Company.

Khaksar, A., C.M. Griffiths, and C. McCann, 1999, Compressional- and shear-wave velocities as a function of confining stress in dry sandstones: *Geophysical Prospecting*, v. 47, p. 487-508.

Kulstad, R.O., 1959, Thickness and salt percentage of the Hutchinson salt; *in* Symposium on Geophysics in Kansas: Kansas Geological Survey Bulletin 137, p. 241-247.

McGuire, D., and B. Miller, 1989, The utility of single-point seismic data; *in* Geophysics in Kansas, D.W. Steeples, ed.: Kansas Geological Survey Bulletin 226, p. 1-8.

Merriam, D.F., 1963, The Geologic History of Kansas: Kansas Geological Survey Bulletin 162, 317 p.

Merriam, D.F., and C.J. Mann, 1957, Sinkholes and related geologic features in Kansas: *Transactions of the Kansas Academy of Science*, v. 60, p. 207-243.

Miller, R.D., 2011, Progress report: 3-D passive surface-wave investigation of solution mining voids in Hutchinson, Kansas: Interim report to Burns & McDonnell Engineering Company, January, 9 p.

Miller, R.D., J. Ivanov, S.D. Sloan, S.L. Walters, B. Leitner, A. Rech, B.A. Wedel, A.R. Wedel, J.M. Anderson, O.M. Metheny, and J.C. Schwarzer, 2009, Shear-wave study above Vigindustries, Inc. legacy salt jugs in Hutchinson, Kansas: Kansas Geological Survey Open-file Report 2009-3.

Park, C., R. Miller, D. Laflen, N. Cabrillo, J. Ivanov, B. Bennett, and R. Huggins, 2004, Imaging dispersion curves of passive surface waves [Exp. Abs.]: Annual Meeting of the Soc. of Expl. Geophys., Denver, Colorado, October 10-15, p. 1357-1360.

Peterie, S.L., M. Tamburro, J. Ivanov, R.D. Miller, B. Wedel, C. Umbrell, and C. Bunker, 2025, Time-lapse vertical seismic profiling in well 2A at the CBRA: Kansas Geological Survey Open-File Report 2025–48.

Sayers, C.M., 2004, Monitoring production-induced stress changes using seismic waves [Exp. Abs.]: Annual Meeting of the Soc. of Expl. Geophys., Denver, Colorado, October 10-15, p. 2287-2290.

Sloan, S.D., S.L. Peterie, J. Ivanov, R.D. Miller, and J.R. McKenna, 2010, Void detection using near-surface seismic methods; *in* Advances in Near-Surface Seismology and Ground-Penetrating Radar, SEG Geophysical Developments Series No. 15, R.D. Miller, J.D. Bradford, and K. Holliger, eds.: Tulsa, Society of Exploration Geophysicists, p. 201-218.

Swineford, A., 1955, Petrography of upper Permian rocks in south-central Kansas: State Geological Survey of Kansas Bulletin 111, 179 p.

Walters, R.F., 1978, Land subsidence in central Kansas related to salt dissolution: Kansas Geological Survey Bulletin 214, 82 p.

Whittemore, D.O., 1989, Geochemical characterization of saltwater contamination in the Macksville sink and adjacent aquifer: Kansas Geological Survey Open-file Report 89-35.

Whittemore, D.O., 1990, Geochemical identification of saltwater contamination at the Siefkes subsidence site: Report for the Kansas Corporation Commission.

Appendix

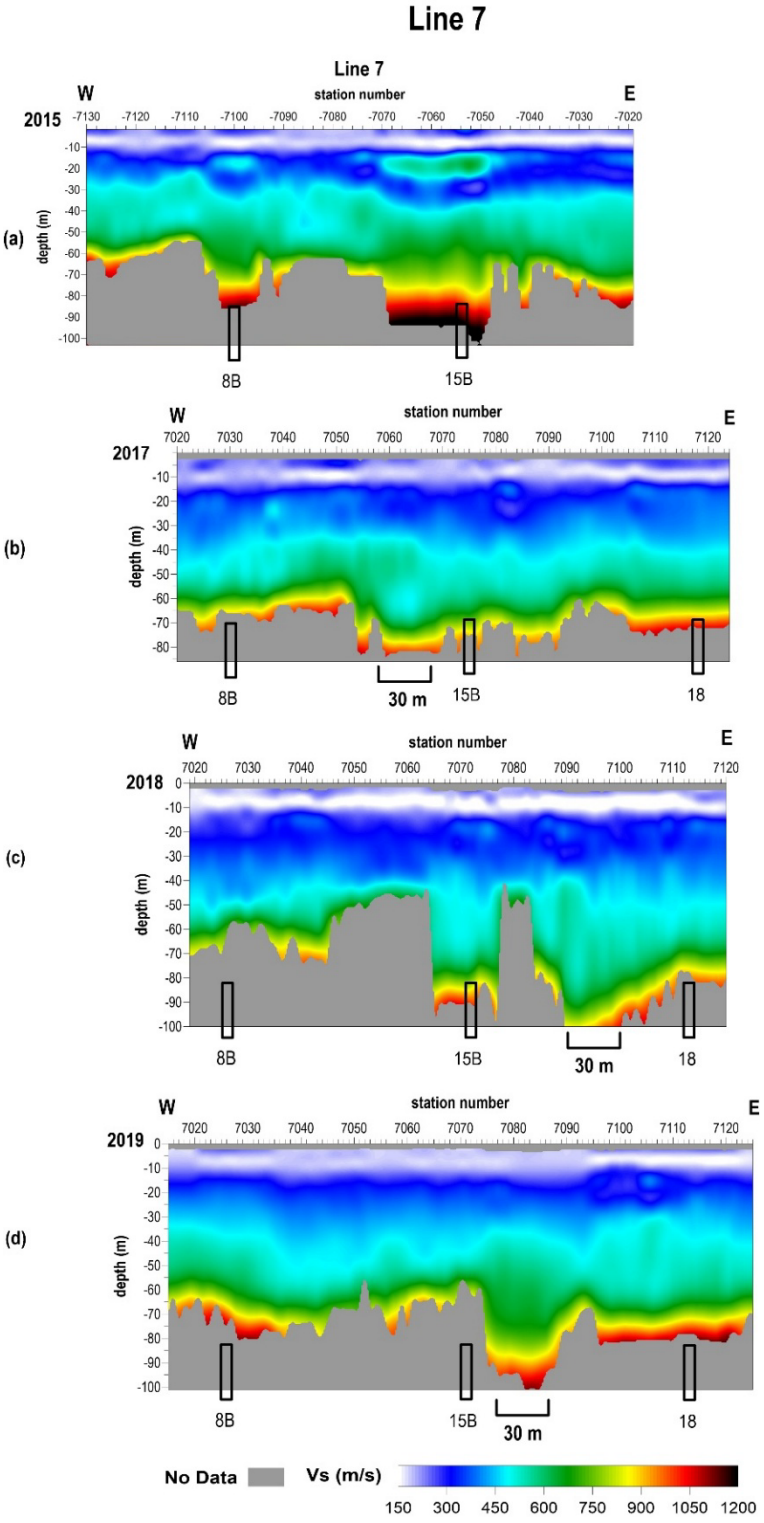

Figure A-1. Shear wave velocity profiles from line 7 in proximity to well 15B for 2015-2019.

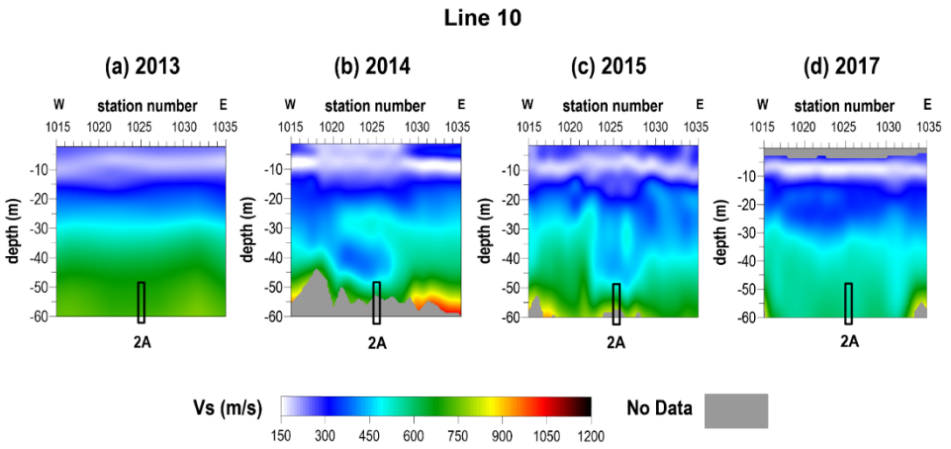

Figure A-2. Shear wave velocity profiles for line 10 over well 2A for 2013-2017.